Structural and functional analyses explain Pea KAI2 receptor diversity and reveal stereoselective catalysis during signal perception

Angelica M Guercio, Salar Torabi, David Cornu, Marion Dalmais, Abdelhafid Bendahmane, Christine Le Signor, Jean-Paul Pillot, Philippe Le Bris, François-Didier Boyer, Catherine Rameau, et al.

communications biology

ARTICLE

https://doi.org/10.1038/s42003-022-03085-6 OPEN

Structural and functional analyses explain Pea KAI2 receptor diversity and reveal stereoselective catalysis during signal perception

Angelica M. Guercio [1], Salar Torabi[2], David Cornu[3], Marion Dalmais[4], Abdelhafid Bendahmane[4], Christine Le Signor[5], Jean-Paul Pillot[6], Philippe Le Bris[6], François-Didier Boyer [7], Catherine Rameau[6], Caroline Gutjahr [2], Alexandre de Saint Germain [6✉] & Nitzan Shabek [1✉]

KAI2 proteins are plant α/β hydrolase receptors which perceive smoke-derived butenolide signals and endogenous, yet unidentified KAI2-ligands (KLs). The number of functional KAI2 receptors varies among species and KAI2 gene duplication and sub-functionalization likely plays an adaptative role by altering specificity towards different KLs. Legumes represent one of the largest families of flowering plants and contain many agronomic crops. Prior to their diversification, KAI2 underwent duplication resulting in KAI2A and KAI2B. Here we demonstrate that *Pisum sativum* KAI2A and KAI2B are active receptors and enzymes with divergent ligand stereoselectivity. KAI2B has a higher affinity for and hydrolyses a broader range of substrates including strigolactone-like stereoisomers. We determine the crystal structures of PsKAI2B in apo and butenolide-bound states. The biochemical, structural, and mass spectra analyses of KAI2s reveal a transient intermediate on the catalytic serine and a stable adduct on the catalytic histidine, confirming its role as a bona fide enzyme. Our work uncovers the stereoselectivity of ligand perception and catalysis by diverged KAI2 receptors and proposes adaptive sensitivity to KAR/KL and strigolactones by KAI2B.

[1] Department of Plant Biology, College of Biological Sciences, University of California, Davis, CA 95616, USA. [2] Plant Genetics, TUM School of Life Sciences, Technical University of Munich (TUM), 85354 Freising, Germany. [3] Université Paris-Saclay, CEA, CNRS, Institute for Integrative Biology of the Cell (I2BC), 91198 Gif-sur-Yvette, France. [4] Institute of Plant Sciences Paris-Saclay, INRAE, CNRS, Université Paris-Saclay, 91405 Orsay, France. [5] Agroecologie, AgroSup Dijon, INRAE, Université Bourgogne Franche Comte, 21000 Dijon, France. [6] Institut Jean-Pierre Bourgin, INRAE, AgroParisTech, Université Paris-Saclay, 78000 Versailles, France. [7] Université Paris-Saclay, CNRS, Institut de Chimie des Substances Naturelles, UPR 2301, 91198 Gif-sur-Yvette, France. ✉email: Alexandre.De-Saint-Germain@inrae.fr; nshabek@ucdavis.edu

Karrikins (KARs) are a family of butenolide small molecules produced from the combustion of vegetation and are bioactive components of smoke[1–3]. These molecules are capable of inducing germination of numerous plant species, even those not associated with fire or fire-prone environments such as Arabidopsis[1–6]. Through studies in Arabidopsis, KAR sensitivity was shown to be dependent on three key proteins: a KAR receptor α/β hydrolase KARRIKIN INSENSITIVE2 (KAI2), an F-box MORE AXILLARY GROWTH 2 (MAX2) component of the Skp1-Cullin-F-box (SCF) E3 ubiquitin ligase, and the target of ubiquitination and degradation, the transcriptional corepressor SMAX1/SMXL2[7–11]. An increasing number of studies shows that the KAR signaling components are involved in the regulation of a number of plant developmental processes including seedling development, leaf shape, cuticle formation, and root development[8,12–15]. Furthermore, they play critical roles in arbuscular mycorrhizal (AM) symbiosis and abiotic stress response[16–18].

The striking similarities between KAR and strigolactone (SL) signaling pathways have been the focus of an increasing number of studies. Both SLs and KARs share a similar butenolide ring structure but instead of the KAR pyran moiety, the butenolide is connected via an enol ether bridge to either a tricyclic lactone (ABC rings) in canonical SLs, or to a structural variety in non-canonical SLs[19,20]. The receptor for SL, DWARF14 (D14) shares a similar α/β hydrolase fold as KAI2 and a parallel signaling cascade requiring the function of the MAX2 ubiquitin ligase and degradation of corepressors (SMXL6, 7 and 8), which belong to the same protein family as SMAX1/SMXL2[7,8,11,21]. Unlike KARs, SLs are plant hormones that act endogenously, but were also found to be exuded by plant roots. SLs affect diverse responses such as hyphal branching of AM fungi to enhance the efficiency of root colonization, germination of root parasitic plant species, shoot branching, lateral root formation, primary root growth, secondary growth in the stem, leaf senescence, and adventitious root formation[22–28]. Notably, KAI2 family receptors have undergone numerous duplication events within various land plant lineages. D14 was found to be an ancient duplication in the KAI2 receptor in the seed plant lineage followed by sub-functionalization of the receptor, enabling SL perception[29–32]. This sub-functionalization has been highlighted by the observations that D14 and KAI2 are not able to complement each other's functions in planta[33–37]. While the role of the D14 receptor in SL signaling is better established, KAI2 receptors and KAR signaling are less understood. A central question in receptor diversity has been the evolutionary purpose and functional significance of *KAI2* duplication and maintenance of the duplicated genes, including but not limited to the duplication event that led to the origin of the distinct SL receptors, D14s. D14s and KAI2s contain over a 70% sequence similarity but confer separate functions in plant. Notably, within the KAI2 family the substitution of a few amino acids within the ligand binding site can alter ligand specificity between KAI2 duplicated copies in *Brassica tournefortii* and *Lotus japonicus*[35,38]. Additionally, given that KAR signaling governs diverse developmental processes including those unrelated to fire, KAI2s are thought to perceive endogenous ligands, which remain elusive and tentatively named KAI2-Ligands (KLs)[29,30,37,39]. Therefore, the ability to alter the specificity of KAI2 receptors to different ligands is likely to be correlated to their ability to perceive distinct KLs. Thus far, several crystal structures of KAI2/D14 receptors have been reported and led to a greater understanding of receptor-ligand perception towards certain ligands[9,21,32,34,40–42]. However, the divergence between duplications of KAI2 receptors to confer altered ligand perception and hydrolysis specificities has been only partially addressed for few plant species at the physiological and biochemical level, and a detailed structural examination is still missing[34–36,38].

Legumes represent one of the largest families of flowering plants and contain many essential crops. Beyond their agronomic value, most legume species are unique among plants because of their ability to fix nitrogen by utilizing symbiosis with rhizobia, in addition to AM symbiosis. Because of the potential functional diversification and specialization of KAI2-ligands, in this study, we examined the physiological and biochemical functions of divergent KAI2 receptors in a legume, using *Pisum sativum (Ps)* as a model. We found that *Pisum sativum* expresses three distinct *KAI2* homologs, two of which, *KAI2A* and *KAI2B* have sub-functionalized, while *KAI2C* is a pseudogene. Using comprehensive biochemical characterization, we show that these divergent receptors display distinct ligand sensitivities and hydrolytic activities. We further substantiate these findings *in planta* by investigating the sensitivities to ligands on hypocotyl elongation in Arabidopsis transgenic complementation lines expressing PsKAI2A and PsKAI2B, as well as studying phenotypic effects in *Pisum sativum* wild-type and *kai2* mutants. Strikingly, KAI2B, was more reactive than KAI2A towards SL/KARs stereoisomers. The diverged receptor was able to cleave the strigolactone synthetic analog (+)-GR24, although not to the same extent as D14/RMS3, suggesting that PsKAI2B evolved the ability to sense SL-like ligands. To further address this point, we determined the structure of an evolutionarily diverged PsKAI2B in *apo* and a unique butenolide-bound state at high resolution (1.6 Å and 2.0 Å, respectively). Unlike the D14 α/β hydrolase, mass spectrometry analysis and structural examination reveal a mode of ligand perception and hydrolysis by PsKAI2B, that involves an intermediate step in which the catalytic serine is transiently bound to a moiety of the ligand and then forms a stable adduct with the catalytic histidine. Altogether, in this study we identified and characterized divergent KAI2 receptors in pea, revealed their distinct function and ligand sensitivities, and illuminated the KAI2s enzymatic mechanism. To this end we have garnered a better understanding of the evolution of plant α/β hydrolase receptors and their functional adaptation in KAR/KL/SL sensing, in particular in a key crop.

Results

Identification and characterization of the Pisum sativum KAI2 genes. To characterize the karrikin sensing machinery in legumes, we built a phylogenetic tree of representative legume *KAI2s*. *KAI2* has undergone two independent duplication events in the legume lineage prior to its diversification followed by the loss of KAI2C in the hologalegina clade resulting in distinct KAI2A and KAI2B protein receptors (Fig. 1a and Supplementary Fig. 1)[38]. We focused on the hologalegina representative *Pisum sativum* for which a high-quality, annotated genome sequence has been recently obtained[43]. We identified three *KAI2* homologs in the pea genome[43] that clearly group within the core KAI2 clade by phylogenetic analysis. One (Psat4g083040) renamed *PsKAI2B*, grouped in the same subclade as the legume *KAI2B*s (including *Lotus japonicus, Lj, KAI2B*[38]), and two Psat2g169960 and Psat3g014200 respectively termed *PsKAI2A* and *PsKAI2C*, in the same subclade as the legume *KAI2A*s (including *LjKAI2A*[38]) (Fig. 1a and Supplementary Fig. 1). *PsKAI2C* was detected by PCR in the genomic, but not the cDNA, and appears to be pseudogene because the predicted encoded protein is truncated at 128 amino acids (aa) due to a premature stop codon at 387 nucleotides after the translation initiation site (Fig. 1b, Supplementary Fig. 2d). By cloning the *PsKAI2A* coding sequence (CDS) we identified two transcripts for this gene, corresponding to two splice variants (Fig. 1b and Supplementary Fig. 2). The transcript PsKAI2A.1 results from intron splicing and encodes a protein of

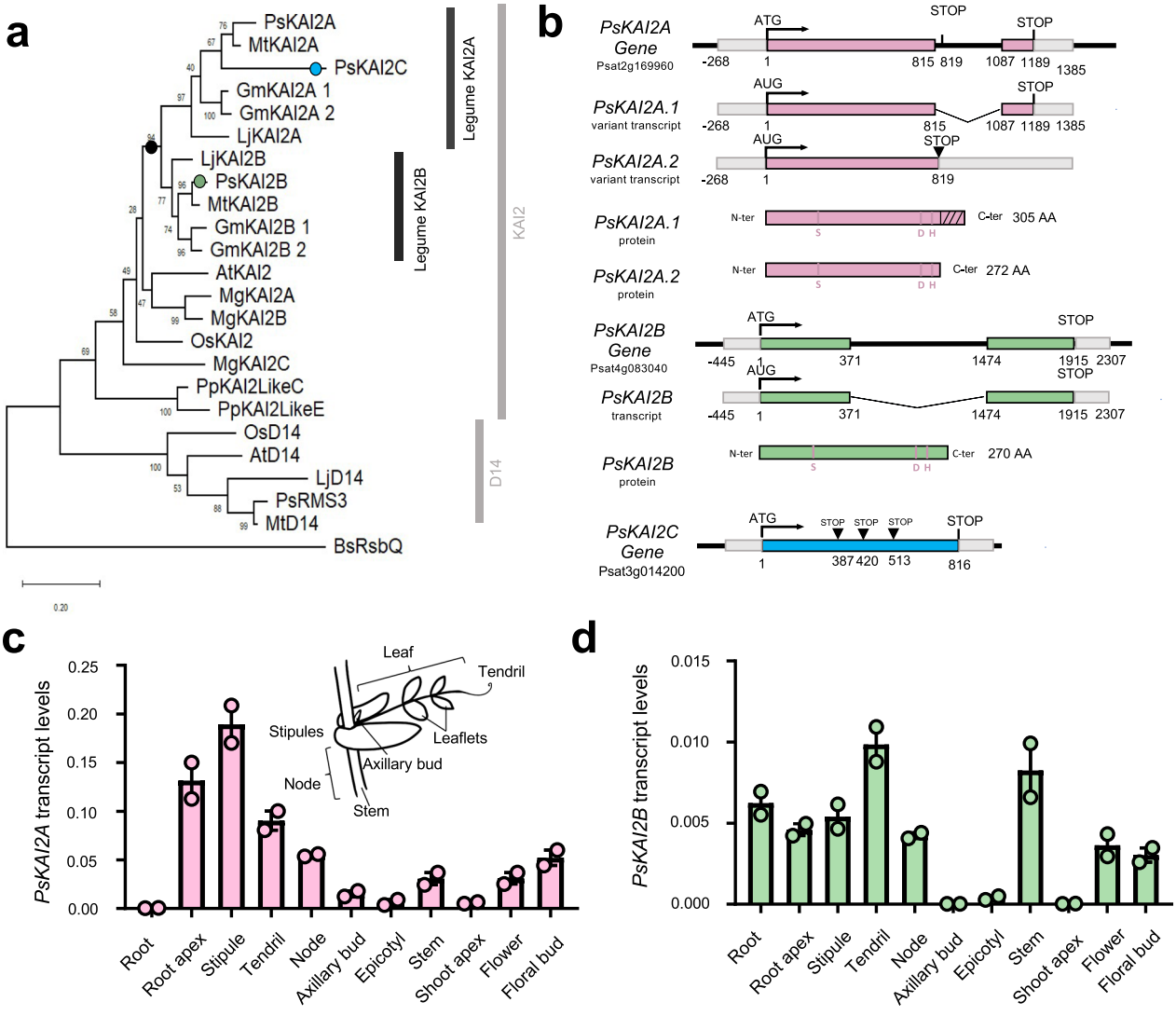

Fig. 1 Evolutionary analysis and differential expression of the legume Pisum sativum KAI2s. a Maximum likelihood phylogeny of 24 representative KAI2 amino acid sequences. Node values represent percentage of trees in which the associated taxa clustered together. Vertical rectangles highlight distinct KAI2 family clades. Black circle indicates legume duplication event. Pink, green, and blue circles mark the position of PsKAI2As, PsKAI2B, and PsKAI2C respectively. The tree is drawn to scale, with branch lengths measured in the number of substitutions per site. **b** PsKAI2A, PsKAI2B and PsKAI2C are homologs to AtKAI2 and encode α-β/hydrolases. Schematic representation of the PsKAI2A, PsKAI2B and PsKAI2C genes; Exons are in pink, green and blue lines, non-coding sequences colored in thin black lines and UTR regions shown as thick gray lines. Bases are numbered from the start codon. PsKAI2A shows 2 splicing variants. Spliced introns are shown as bent ("V") lines. Inverted triangle (▼) indicates premature termination codons. Catalytic triad residues are indicated in pink. The hatched part indicated the C-terminus extension of the PsKAI2.1 protein (**c**, **d**) Differential expression pattern of PsKAI2A (**c**, pink) and PsKAI2B (**d**, green). Transcript levels in the different tissues of 21 old wild-type Pisum sativum plants (cv. Terese) were determined by real-time PCR, relative to PsEF1α. Data are means ± SE ($n = 2$ pools of 8 plants). Inset drawing of a node showing the different parts of the pea compound leaf.

305 aa. Thus, this protein shows a C-terminal extension of 33 aa similar to LjKAI2A (Supplementary Fig. 2), missing in other KAI2 proteins. The PsKAI2A.2 transcript arises from the intron retention and shows a premature STOP codon two nucleotides after the end of the first exon. This leads to a 272 aa protein representing a similar size to other KAI2s described (Fig. 1b and Supplementary Fig. 2). Due to the similar size, lack of introns, and evolutionary conservation of the residues contained in the PsKAI2A.2 protein, PsKAI2A hereafter will refer to the PsKAI2A.2 protein. From this analysis, it is clear that the KAI2 clade has undergone an independent duplication event in the legume lineage, resulting in two functional forms: KAI2A and KAI2B (Supplementary Fig. 1a-b). To examine potential functional divergence between PsKAI2A and PsKAI2B, we first analyzed the aa sequences and identified notable alterations in key residues, of which numerous are likely to be functional changes as indicated in later analyses (Supplementary Fig. 3). To further characterize divergence of these genes, we studied their expression patterns in various tissues of the *Pisum* plant (Supplementary Fig. 1c-d). Interestingly, *PsKAI2A* was ten-fold more highly expressed in comparison to *PsKAI2B* and the expression in the roots differed between the two forms, suggesting sub-functionalization between transcriptional regulatory sequences of *PsKAI2A* and *PsKAI2B*.

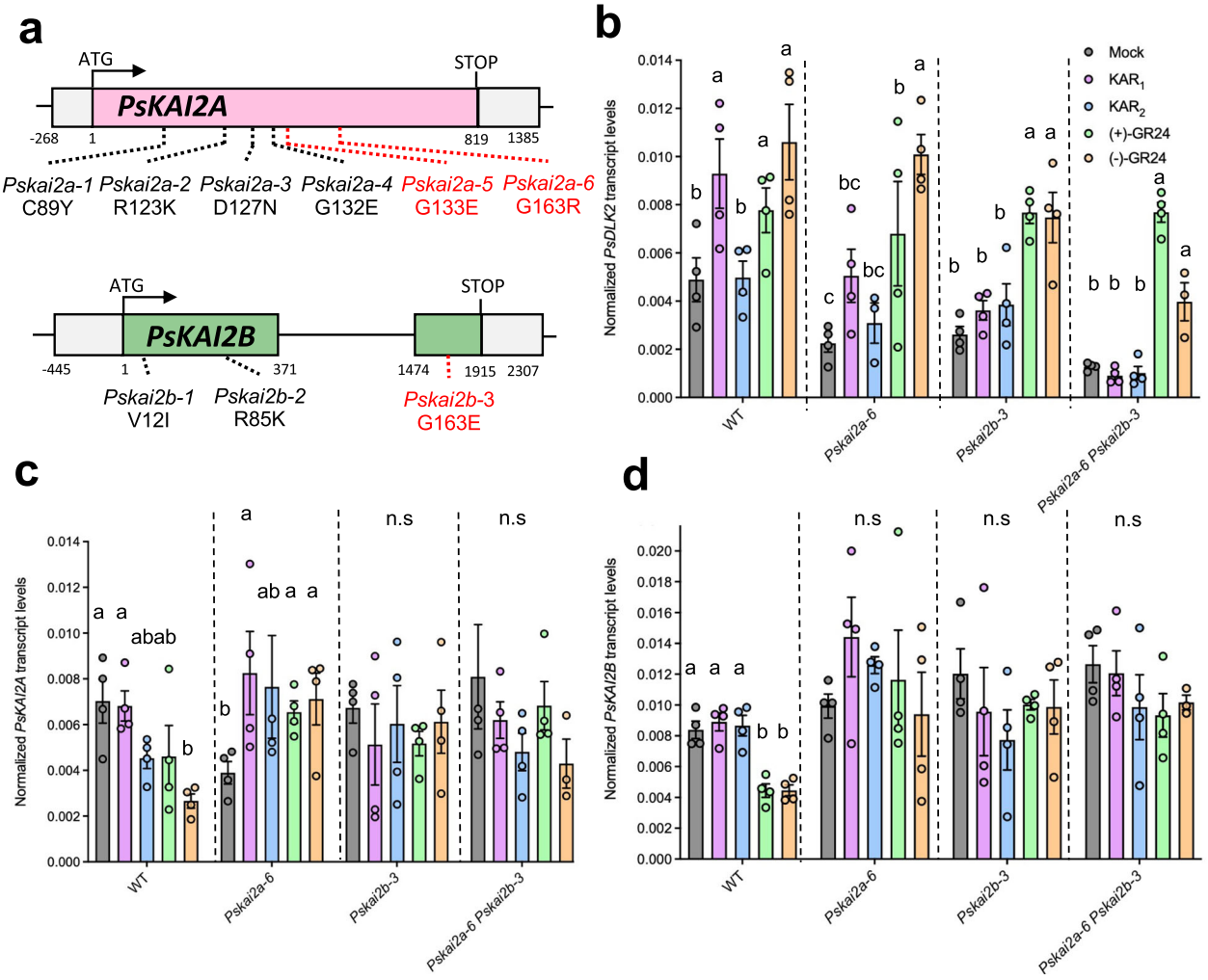

Fig. 2 Characterization of the *Pskai2* mutants. a Gene structure of *PsKAI2* and locations of mutations. Bases are numbered from the start codon. Point mutations are indicated by dotted lines (black and red for the one studied here). RT-qPCR-based expression of *PsDLK2* (**b**), *PsKAI2A* (**c**), *PsKAI2B* (**d**) in roots of 10 day old *P. sativum* plants after 4 h treatment with solvent (Mock) or 3 µM KAR_1 OR KAR_2 or (+)-GR24 or (−)-GR24. Expression values were normalized to those of the housekeeping gene *TUBULIN* ($n = 3$–4). **a**–**c** Letters indicate significant differences versus mock treatment (Kruskal-Wallis Test, $p < 0.05$).

Identification and phenotypic examination of Pskai2a and Pskai2b TILLING mutants. To investigate the function of *PsKAIA* and *PsKAI2B*, mutants in both genes were identified via Targeting-Induced Local Lesions IN Genomes (TILLING) using the mutagenized Caméor population[44,45]. Twenty mutations in *PsKAI2A* and sixteen mutations is *PsKAI2B* were identified (Supplementary Table 1). Among them, six of the *PsKAI2A* and three of the *PsKAI2B* mutations were predicted as non-synonymous and based on their position may result in mutated amino acids that compromise the protein function (Supplementary Table 1, Fig. 2a, Supplementary Fig. 4). The comparison between wild-type and *Pskai2* single mutants revealed a slight reduced plant height for *Pskai2a-6 and Pskai2b-3*, a phenotype which is stronger for the double mutants *Pskai2a-5 Pskai2b-3 and Pskai2a6 Pskai2b-3*. No strong differences in branch length were observed despite branching at node 2 was reduced for *Pskai2b-3* and *Pskai2a-5 Pskai2b-3*, which is in contrast to SL receptor mutants which show an increase in branching[22–28]. In pea, branching at node 2 is rather qualitative and the number of plants with a long branch at this node on 12 plants (>50 mm) was 8 for WT, 11 and 8 for *Pskai2a-6* and *Pskai2a-5*, respectively, and 4 and 2 for *Pskai2b-3* and *Pskai2a-5 Pskai2b-3*, respectively (Supplementary Fig. 5a-c). Similar to the other legume *L. japonicus* and in contrast to *Arabidopsis thaliana*[38,46], the root hair length of the double mutant *Pskai2a-6 Pskai2b-3* in pea was not significantly different from wild-type. Together, under our growth conditions, KAI2 requirement for root hair elongation differs among plant species/families and may be absent from legumes. (Supplementary Fig. 5d, e).

Karrikin signaling reporter DLK2 expression is mediated by KAI2s in P. sativum roots in a ligand-specific manner. To examine the activation of the Karrikin signaling pathway by PsKAI2s, we monitored the expression levels of the downstream gene *D14-LIKE 2* (*DLK2*). Perception of the small molecule signal by KAI2 has been shown to induce expression of transcripts including *DLK2*, which is commonly used as the main KAR-signal reporter gene[35,37,38,47]. It was recently shown, in *L. japonicus* that the root system architecture can be modulated by KAR_1 but not by KAR_2 treatment, and likewise the expression of the KAR signaling marker gene, *DLK2* in roots, was responsive only to KAR_1 but not to KAR_2[38]. Furthermore, LjKAI2A and LjKAI2B have distinct ligand-binding specificities since LjKAI2A but not LjKAI2B can perceive (−)-GR24 in vitro. This alteration in perception depends on the divergent amino acid F157/W158 within the ligand binding pocket, and indeed in roots, LjKAI2A but not

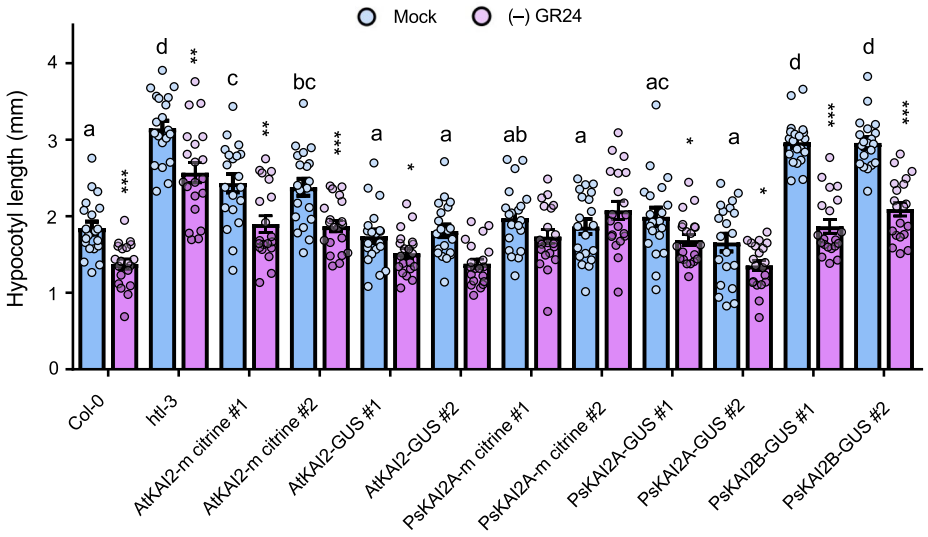

Fig. 3 Arabidopsis hypocotyl elongation complementation assays with PsKAI2s. Hypocotyl length of 7-day-old seedlings grown under low light at 21 °C. Data are means ± SE ($n = 20$–24; 2 plates of 10-12 seedlings per plate). Light blue bars: Mock (DMSO), lavender bars: (–)-GR24 (1 µM). Complementation assays using the AtKAI2 promoter to express AtKAI2 (control) or PsKAI2 genes in the htl-3 mutant background (Col-0 ecotype) as noted above the graph. Proteins were tagged with mCitrine or GUS protein. For DMSO controls, statistical differences were determined using a one-way ANOVA with a Tukey multiple comparison of means post-hoc test, statistical differences of $p < 0.05$ are represented by different letters. Means with asterisks indicate significant inhibition compared to mock-treated seedlings with *** corresponding to $p \leq 0.0001$, ** corresponding to ≤0.001 and * to $p \leq 0.01$, as measured by t test.

LjKAI2B can induce *DLK2* expression in response to (–)-GR24[38]. Intriguingly, because the F157/W158 amino acid difference between KAI2A and KAI2B is not conserved across most legumes including pea, this raises the question how pea roots respond to the range of artificial ligands. Thus, we treated pea wild-type, *kai2a-6, kai2b-3, and kai2a-6 kai2b-3* double mutant roots with KAR_1, KAR_2, (+)-GR24, and (–)-GR24 and performed RT-qPCR analysis of *PsDLK2* transcript accumulation (Fig. 2b). Without treatment, *PsDLK2* expression was significantly reduced in both single mutants (*kai2a-6* and *kai2b-3*) indicating that *KAI2A* and *KAI2B* are not fully redundant. Consistently, *DLK2* expression was further reduced in the double mutant (*kai2a-6 kai2b-3*) (Fig. 2b). This expression pattern strongly suggests that PsKAI2A and PsKAI2B function in KL signaling and validates that the *kai2a-6* and *kai2b-3* mutants perturb protein function. Induction of *DLK2* in response to karrikins was similar to *L. japonicus*, as in the wild-type, it was showed higher transcript accumulation after KAR_1-treatment but no response to KAR_2-treatment. In the mutants KAR_1 evoked only a slight *PsDLK2* response in *Pskai2a-6*, whereas *Pskai2b-3* showed no *PsDLK2* induction, similar to the double mutant. Given that both *PsKAI2A* and *PsKAI2B* transcripts accumulated to similar levels (Fig. 2c, d), these data suggest either that PsKAI2B protein accumulates to higher levels than PsKAI2A, or it is more active in KAR_1 perception. Consistent with the wild-type, the mutants did not respond to KAR_2. In all genotypes, *PsDLK2* was induced by treatment with (+)-GR24, the ligand of D14. Unlike the observations with *L. japonicus*[38], all pea genotypes also showed a significantly increased *DLK2* transcript accumulation in response to (–)-GR24, with a significantly stronger induction shown in the wild-type and the single mutants as compared to the double mutant. Thus, in pea, (–)-GR24 is not only perceived by KAI2 but to some extent also by the SL receptor D14, similar to previous observations in Arabidopsis[46]. However, we cannot exclude the possibility that the mutated proteins are still able to perceive (–)-GR24, even though they lost sensitivity to KAR_1. Unfortunately, although *DLK2* is a good marker gene for KAI2-mediated signaling, it also responds to D14-mediated signaling[35,37,38,47]. No specific marker gene for KAI2-mediated signaling is available to date, but the insights into the differential signaling of PsKAI2A and PsKAI2B remain highly informative.

PsKAI2A, but not PsKAI2B, rescues inhibition of hypocotyl elongation in Arabidopsis kai2 mutants. Since we could not distinguish a possible differential sensitivity of PsKAI2A and PsKAI2B in the pea background (as previously observed in *L. japonicus*[38]), we performed a cross-species complementation by transforming the Arabidopsis *htl-3* (also known as *kai2*) mutant with *PsKAI2A* and *PsKAI2B* (Fig. 3). The genes were expressed as fusions with *mCitrine* or *GUS* and driven by the native *AtKAI2* promoter (p*AtKAI2*) (Supplementary Fig. 6). To test protein functionality we performed the widely used hypocotyl elongation assay[33,39] under low light conditions, which causes an elongated hypocotyl phenotype of the *htl-3* mutant when compared to the wild-type Columbia (Col-0). Remarkably, all transgenes, except *PsKAI2B*, completely or partially restored hypocotyl length of *htl-3* to the wild-type length (Fig. 3). Furthermore, all lines (even *htl-3*), except those complemented with PsKAI2A responded to (-)-GR24 (Fig. 3). We repeated the complementation for the *kai2-2* mutant in the Landsberg erecta (Ler) background. This confirmed that the two *PsKAI2A* splice forms restore the reduced hypocotyl length in *kai2-2* but the proteins did not mediate responses to (–)-GR24. In contrast, PsKAI2B did not restore the wild-type hypocotyl length but mediated a response to (–)-GR24 (Supplementary Fig. 6). These results suggest that PsKAI2A can perceive endogenous Arabidopsis KL(s) but does not perceive the synthetic (-)-GR24. In contrast, PsKAI2B is unable to perceive endogenous Arabidopsis KL(s) but is sensitive to (-)-GR24. This further suggests that *PsKAI2A* may be the functional orthologue

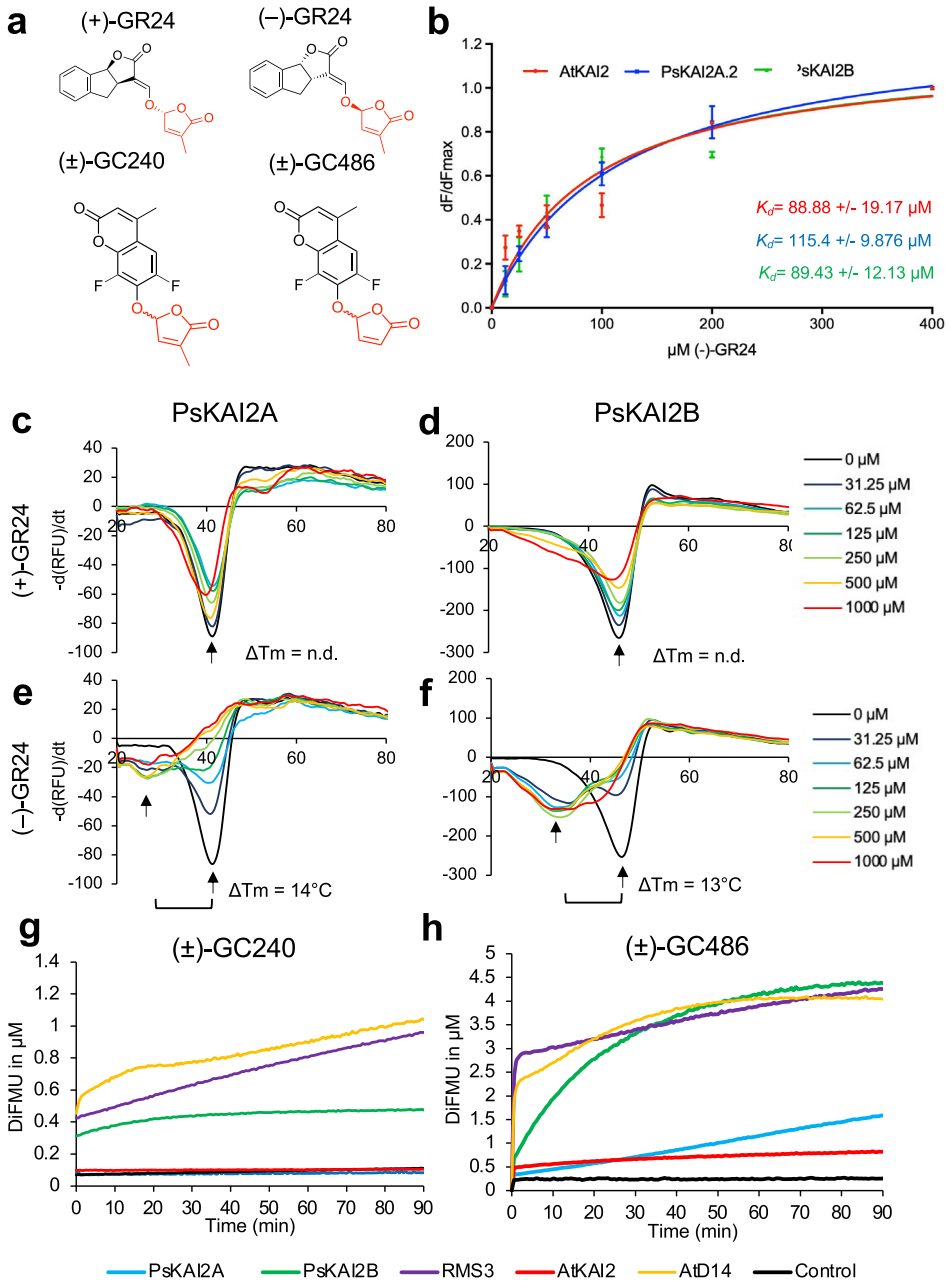

Fig. 4 Biochemical analysis of PsKAI2A and PsKAI2B interactions with different GR24 isomers and enzymatic property. a Chemical structure of ligands used. **b** Plots of fluorescence intensity *versus* SL concentrations. The change in intrinsic fluorescence of AtKAI2, PsKAI2A and PsKAI2B was monitored (see Supplementary Fig. 9) and used to determine the apparent K_d values. The plots represent the mean of two replicates and the experiments were repeated at least three times. The analysis was performed with GraphPad Prism 7.05 Software. DSF assay. The melting temperature curves of 10 µM PsKAI2A (**c**, **e**) or PsKAI2B (**d**, **f**) with (+)-GR24 (**c**, **d**), (-)-GR24 (**e**–**f**) at varying concentrations are shown as assessed by DSF. Each line represents the average protein melt curve for three technical replicates; the experiment was carried out twice. Enzymatic kinetics for AtD14, AtKAI2, RMS3, PsKAI2A and PsKAI2B proteins incubated with (±)-GC240 (**g**) or (±)-GC486 (**h**). Progress curves during probes hydrolysis, monitored (λ_{em} 460 nm) at 25 °C. Protein catalyzed hydrolysis with 400 nM µM of protein and 20 µM of probes. These traces represent one of the three replicates and the experiments were repeated at least two times.

of Arabidopsis *KAI2* while PsKAI2B has diverged and adapted to perceive different ligands, possibly those important for processes unique to legumes.

Altered ligand binding specificity and activity between PsKAI2s. To further investigate the distinct ligand selectivity, we purified PsKAI2 recombinant proteins and studied their ligand-interaction and ligand-enzymatic activities using various complementary assays (Figs. 4–5 and Supplementary Fig. 7–9). We first examined PsKAI2A and PsKAI2B ligand interactions via the thermal shift assay (Differential Scanning Fluorimetry, DSF) with various KAI2/D14 family ligands including (+) and (−)-GR24 enantiomers (also known as $GR24^{5DS}$ and $GR24^{ent\text{-}5DS}$, respectively), and (+)- and (−)-2'-*epi*-GR24 (also known as $GR24^{4DO}$ and $GR24^{ent\text{-}4DO}$ respectively)[48] (Fig. 4c–f, Supplementary Fig. 8). DSF is a method used to detect changes in stability of proteins, in this case via the addition of a ligand[49]. DSF

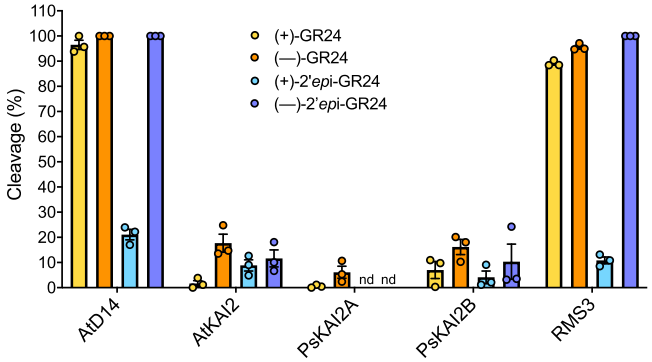

Fig. 5 Comparative enzymatic activity of AtD14, AtKAI2, RMS3, PsKAI2A and PsKAI2B proteins with GR24 isomers. UPLC-UV (260 nm) analysis showing the formation of the ABC tricycle from GR24 isomers. The enzymes (10 µM) hydrolysis activity was monitored after incubation with 10 µM (+)-GR24 (yellow), (-)-GR24 (orange), (+)-*2′-epi*-GR24 (blue), or (-)- *2′-epi*-GR24 (purple). The indicated percentage corresponds to the hydrolysis rate calculated from the remaining GR24 isomer, quantified in comparison with indanol as an internal standard. Data are means ± SE ($n = 3$). nd = no cleavage detected.

analyses revealed an increased shift in stability in the presence of (−)-GR24 for PsKAI2B as compared to PsKAI2A which displayed only little alteration (Fig. 4c–f). The other ligands and enantiomers induced no detectable shift in stability for either receptor. An extensive interaction screen using intrinsic fluorescence confirmed that only the (−)-GR24 stereoisomer interacted with PsKAI2 proteins (Fig. 4b and Supplementary Fig. 9), and further corroborated the results of the Arabidopsis hypocotyl elongation and the DSF assays. The calculated K_d showed a higher affinity for (−)-GR24 for PsKAI2B ($K_d = 89.43 \pm 12.13$ µM) than PsKAI2A ($K_d = 115.40 \pm 9.87$ µM).

Because of the structural similarity between KAI2 and D14 α/β hydrolases, in particular the conserved serine catalytic triad signature of these receptors, we examined the potential catalytic function of KAI2s. The hydrolytic activity of the PsKAI2 proteins towards distinct ligands was quantified in comparison to AtD14, AtKAI2, and RMS3. The proteins were incubated with (+)-GR24, (−)-GR24, (+)-2′-*epi*-GR24 and (−)-2′-*epi*-GR24 in presence of 1-indanol as an internal standard, followed by ultraperformance liquid chromatography (UHPLC)/UV DAD analysis (Fig. 5). Interestingly, PsKAI2A can only cleave (−)-GR24, while PsKAI2B was able to cleave (+)-GR24, (−)-GR24 and (−)-2′-*epi*-GR24 stereoisomers. Among the tested ligands, all enzymes showed reduced activity towards (+)-2′-*epi*-GR24, and among the KAI2s, PsKAI2A had no detectable activity for (+)-2′-*epi*-GR24. These results strongly indicate that PsKAI2s have distinct stereoselectivity, and PsKAI2B appears to be more reactive to ligands shared with AtD14 and RMS3. AtD14 and PsRMS3 (*Pisum* D14) similarly bind and hydrolyze both the isolated (−)- and (+)-GR24 stereoisomers as well as the racemic forms at a higher efficiency than KAI2s as shown previously[33,36,38,48,50]. This is counterintuitive as (−)-GR24 acts more strongly through KAI2 *in planta*[33,36,38,48,50]. Further studies are needed to explain this discrepancy in the future. To further investigate the hydrolysis kinetics of PsKAI2 proteins, we performed an enzymatic assay with pro-fluorescent probes that were previously designed for detecting SL hydrolysis[36,50] (Fig. 4g–h). The pro-fluorescent probes ((±)-GC240) and ((±)-GC486) are SL analogs where the ABC rings are replaced by a fluorophore: a coumarine-derived moiety (DiFMU). When cleaved by D14 and KAI2 proteins, the fluorophore is released which results in an increase in fluorescence, thereby providing a readout of enzymatic activity. As expected, PsKAI2A showed no activity towards the probe (±)-GC240, similar to AtKAI2, as previously reported[36,50]. Strikingly, PsKAI2B was able to cleave (±)-GC240, suggesting yet again that unlike PsKAI2A, PsKAI2B has a ligand stereoselectivity that is more similar to AtD14 and RMS3 than to KAI2A (Fig. 4g). Since probes without a methyl group, such as dYLG, can serve as the hydrolysis substrates for AtKAI2[51], we tested the activity of KAI2s and D14s using the (±)-GC486 probe bearing no methyl-group on the D-ring. Notably, PsKAI2B, RMS3, and AtD14 were able to effectively hydrolyze (±)-GC486, whereas PsKAI2A and AtKAI2 showed little activity (Fig. 4h). Nonetheless, PsKAI2A and AtKAI2 also exhibit a biphasic time course of fluorescence, consisting of an initial phase, followed by a plateau phase. Comparative analysis of the kinetic profiles shows that PsKAI2B, RMS3 and AtD14 display a higher plateau (1 µM versus 0.3 µM of DiFMU, Fig. 4h). Taken together the comparative kinetic analysis substantiates the distinct function of PsKAI2B compared to PsKAI2A not only highlights the similarity of PsKAI2B to SL receptors[8,10,36,40–42,50,52] rather than karrikin receptors[8–10,13,34–36,38,51], but may also offer new insights into the evolution of D14 from KAI2 via intermediate KAI2 versions.

Structural insights into divergence of legume KAI2A and KAI2B. To elucidate the structural basis for the differential ligand selectivity between KAI2A and KAI2B, we determined the crystal structure of PsKAI2B at 1.6 Å resolution (Fig. 6 and Table 1). The PsKAI2B structure shares the canonical α/β hydrolase fold and comprises base and lid domains (Fig. 6a). The core domain contains seven-stranded mixed β-sheets (β1–β7), five α-helices (αA, αB, αC, αE and αF) and five 3_{10} helices (ŋ1, ŋ2, ŋ3, ŋ4, and ŋ5). The helical lid domain (residues 124–195, Supplementary Fig. 3) is positioned between strands β6 and β7 and forms two parallel layers of V-shaped helices (αD1-4) that create a deep pocket area adjoining the conserved catalytic Ser-His-Asp triad site (Fig. 6a and Supplementary Fig. 3). Despite the sequence variation (77% similarity between PsKAI2B and AtKAI2, Supplementary Fig. 3), we did not observe major structural rearrangements between PsKAI2B and the previously determined Arabidopsis KAI2 structure[53] as shown by an Root Mean Squared Deviation (RMSD) of 0.35 Å for superposition of backbone atoms (Fig. 6b). This similarity and the relatively low RMSD values between α/β hydrolase proteins are expected and have been shown for both D14 and KAI2s and even the ancestral α/β hydrolase RBSQ despite their distinct ligand sensitivities[9,21,32,34,53]. Nonetheless, further structural comparative analyses have identified two residue alterations in positions 129 and 147 within the lid domain which appear to slightly alter the backbone atoms and generally distinguish legume KAI2 proteins from KAI2s in other species (Supplementary Fig. 3 and Fig. 6b). The asparagine residue in position 129 is more prevalent in legume KAI2As, and the legume alanine or serine in position 147 has diverged from bulky polar residues compared to other KAI2s. Therefore, it is likely that these amino acids variations may play a role in downstream events rather than directly modulating perception of distinct ligands.

To further determine the differential ligand specificity between PsKAI2A and PsKAI2B, we utilized the PsKAI2B crystal structure reported here to generate a high probability 3D model for PsKAI2A. As expected, PsKAI2A structure exhibits a similar backbone atom arrangement (RMSD of 0.34 Å) that parallels the PsKAI2B structure (Fig. 7a). Nonetheless, we identified eight significant divergent amino acids between the two structures including residues involved in forming the ligand binding pocket as well as solvent-exposed regions (Fig. 7b–d and Supplementary Fig. 10a-b). Because these variants are evolutionarily conserved across legumes, the analysis of the underlined residues not only distinguishes between KAI2A and KAI2B in *Pisum* but can be extrapolated to other legume KAI2A/B diverged proteins.

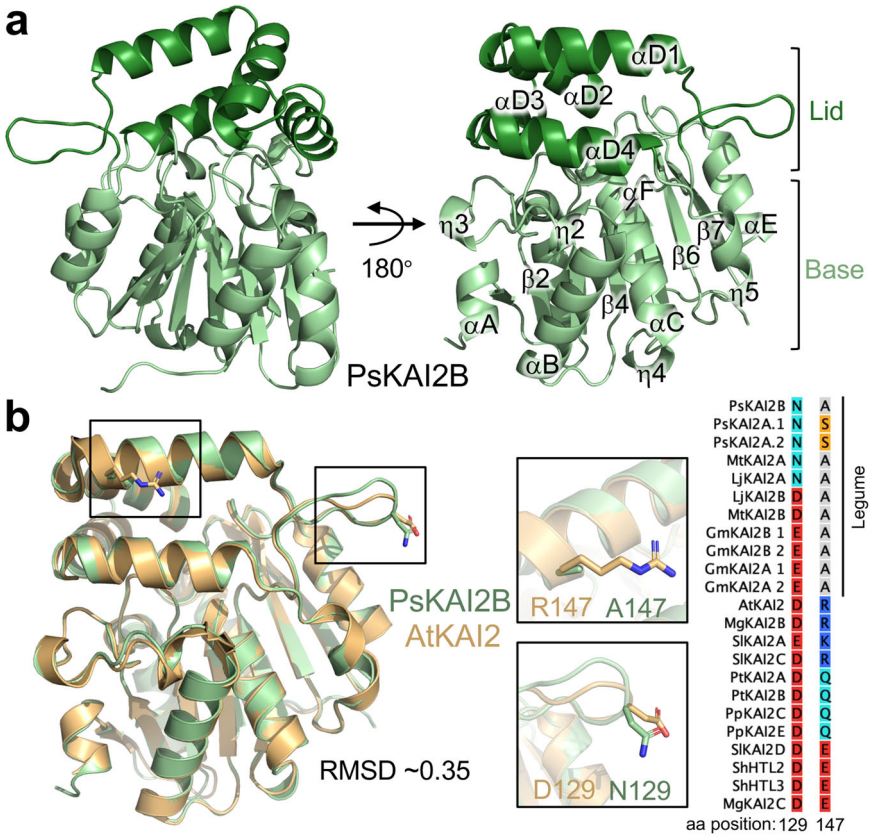

Fig. 6 The crystal structure of legume KAI2. a Overview of PsKAI2B structure. Lid and base domains are colored in forest and light green respectively with secondary structure elements labeled. **b** Structural alignment of PsKAI2B and AtKAI2 (PDB ID: 4HTA) shown in light green and wheat colors respectively. Root-mean-square deviation (RMSD) value of the aligned structures is shown. The location and conservation of legume KAI2 unique residues, alanine in position 147 (A147) and asparagine N129, are highlighted on the structure shown as sticks as well as in reduced Multiple Sequence Alignment from Supplementary Fig. 3.

Structural comparative analysis within the ligand-binding pocket showed divergent solvent accessibility between PsKAI2A and PsKAI2B (Fig. 7b). PsKAI2B exhibits a structural arrangement that results in a larger volume of the hydrophobic pocket (125.4 A^3) yet with a smaller entrance circumference (30.3 Å) than PsKAI2A (114.8 A^3 and 33.6 Å, respectively, Fig. 7b). Further *in silico* docking experiments of (–)-GR24 with PsKAI2B resulted in a successful docking of the ligand that is completely buried in the pocket and positioned in a pre-hydrolysis orientation nearby the catalytic triad. In contrast, docking experiments of (–)-GR24 with PsKAI2A resulted in more restricted interaction with the ligand being partially outside the pocket (Supplementary Fig. 10c). Notably, we found five key residues that directly alter the pocket morphology (Fig. 7c and Supplementary Fig. 10a-b). Among these residues, L160/S190/M218 in PsKAI2A and the corresponding residues, M160/L190/L218 in PsKAI2B are of particular interest because of their functional implications in the pocket volume and solvent accessibility (Fig. 7d). Interestingly, the variant in position 218 places it in the center of the Asp loop (D-loop, region between β 7 and αE, Fig. 7c, d), that has been recently suggested to impact D14 protein-protein interactions in SL signaling[54,55]. Residues 160 and 190 are of great interest because of their direct effect on ligand accessibility and binding pocket size. Residue 160 is positioned at the entrance of the ligand-binding pocket in helix αD2, thus the substitution of leucine (L160 in KAI2A) to methionine (M160 in KAI2B) results in modifying the circumference of PsKAI2B pocket entrance (Fig. 7b–d). While both L160 and M160 represent aliphatic non-polar residues, the relative low hydrophobicity of methionine as well as its higher plasticity are likely to play a major role in modifying the ligand pocket. Residue 190 (S190 in PsKAI2A and L190 in PsKAI2B, Fig. 7d) is positioned in helix αD4 and represents a major structural arrangement at the back of the ligand envelope. Because leucine has moderate flexibility compared to serine and much higher local hydrophobicity, this variation largely attributes to the changes in the pocket volume as well as fine-tunes available ligand orientations.

To further examine whether the diverged residues directly impact ligand perception, we produced the recombinant reciprocal swap mutants $PsKAI2A^{L160M,\ S190L}$ and $PsKAI2B^{M160L,\ L190S}$, and tested their sensitivity to selected ligands by DSF. Remarkably, as can be seen by the ΔTm, the swap of PsKAI2A and PsKAI2B at residues 160 and 190 resulted in a loss of sensitivity of $PsKAI2B^{M160L,\ L190S}$ towards (–)-GR24 ligand, yet with no gain of sensitivity of $PsKAI2A^{L160M,\ S190L}$ (Supplementary Fig. 11a-d). This demonstrates that the variation in residues 160 and 190 in KAI2s are necessary for ligand perception and selectivity but may not be entirely sufficient for PsKAI2B perception of (–)-GR24. Notably, structural analysis of the ligand-envelopes of $PsKAI2A^{L160M,\ S190L}$ and $PsKAI2B^{M160L,\ L190S}$ in comparison to their WT counterparts further corroborates the smaller pocket sizes as well as the inferior docking scores of the swap mutant which can explain the observed loss of sensitivity to (–)-GR24 (Supplementary Fig. 11e–g).

Structural and functional elucidation of ligand hydrolysis mechanism by PsKAI2B receptor. To examine the molecular interaction of PsKAI2B with the enantiomer (–)-GR24, we co-crystallized and determined the structure of PsKAI2B-(–)-GR24

Table 1 Data collection, phasing and refinement statistics.

	PsKAI2B (apo form, with glycerol)	(—)-GR24 D-OH - bound PsKAI2B
Data collection		
Space group	C2	C2
Cell dimensions		
a, *b*, *c* (Å)	87.59, 71.14, 49.06	87.08, 71.82, 48.79
α, β, γ (°)	90, 117, 90	90, 117.3, 90
Resolution (Å)	43.47-1.61 (1.66-1.61)*	43.36-2.00 (2.07-2.00)
R_{sym}	0.080 (0.589)	0.082 (0.316)
$I/\sigma I$	31.01 (1.52)	35.13 (4.11)
Completeness (%)	99.2 (84.5)	98.73 (87.53)
Redundancy	6.4 (3.2)	6.1 (4.5)
Refinement		
Resolution (Å)	1.61	2.00
No. reflections	34306	17837
R_{work} / R_{free} (%)	15.9/17.7	16.9/21.1
No. atoms	2395	2298
Protein	2110	2110
Ligand/ion	6	8
Water	279	180
B-factors		
Protein	19.92	26.5
Ligand/ion	33.73	24.60
Water	32.07	32.22
R.m.s. deviations		
Bond lengths (Å)	0.009	0.013
Bond angles (°)	0.88	1.03
Ramachandran favored (%)	98.51	98.88
Ramachandran allowed (%)	1.49	1.12
Ramachandran outliers (%)	0	0
PDB ID	7K2Z	7K38

*Values in parentheses are for highest-resolution shell.

at 2.0 Å resolution (Fig. 8a and Table 1). Electron density map analysis of the ligand-binding pocket revealed the existence of a unique ring-shaped occupancy that is contiguously linked to the catalytic serine (S95) (Fig. 8a-b). The structural comparison of the backbone atoms between apo-PsKAI2B and PsKAI2B- (–)-GR24 did not reveal significant differences (Supplementary Fig. 12a) and is in agreement with previously reported *apo* and ligand bound D14/KAI2 crystal structures[9,10,21,32,41]. This similarity suggests that a major conformational change may indeed occur as proposed for D14[55]. It may happen after the nucleophilic attack of the catalytic serine and the (–)-GR24 cleavage which is likely to be a highly unstable state for crystal lattice formation. Further analysis suggests that the 5-hydroxy-3-methylbutenolide (D-OH ring), resulting from the (–)-GR24 cleavage, is trapped in the catalytic site (Supplementary Fig. 12b-d). The lack of a defined electron density fitting with the tricyclic lactone (ABC ring) may exclude the presence of the intact GR24 molecule. Other compounds present in the crystallization condition were tested for their ability to occupy the S95-contiguous density, and the D-OH group of (–)-GR24 demonstrated the highest calculated correlation coefficient (CC) score and the best fit in the PsKAI2B co-crystal structure (Supplementary Fig. 12c). Additional tests of D-OH binding including *in silico* docking simulations and analyses revealed a high affinity for D-OH in a specific orientation and in agreement with the structure presented here (Supplementary Fig. 12d). The most probable orientation of the D-OH positions the methyl group (C4') together with the hydroxyl group of D-OH towards the very bottom/back of the pocket near the catalytic serine, where the O5" atom is coordinated by both N atoms of F26 and V96 (Fig. 8b-c). The hemiacetal group (C2') of D-OH is oriented towards the access groove of the pocket with angles (between carbon and oxygen atoms) supporting the captured D-OH in an orientation in which cleavage of the intact (–)-GR24 may have taken place. The C5' of D-OH appears to form a covalent bond with Oγ of S95 (dark gray line in Fig. 8c) and generates a tetrahedral carbon atom. The overall positioning of this molecule is strictly coordinated by F26, H246, G25, and

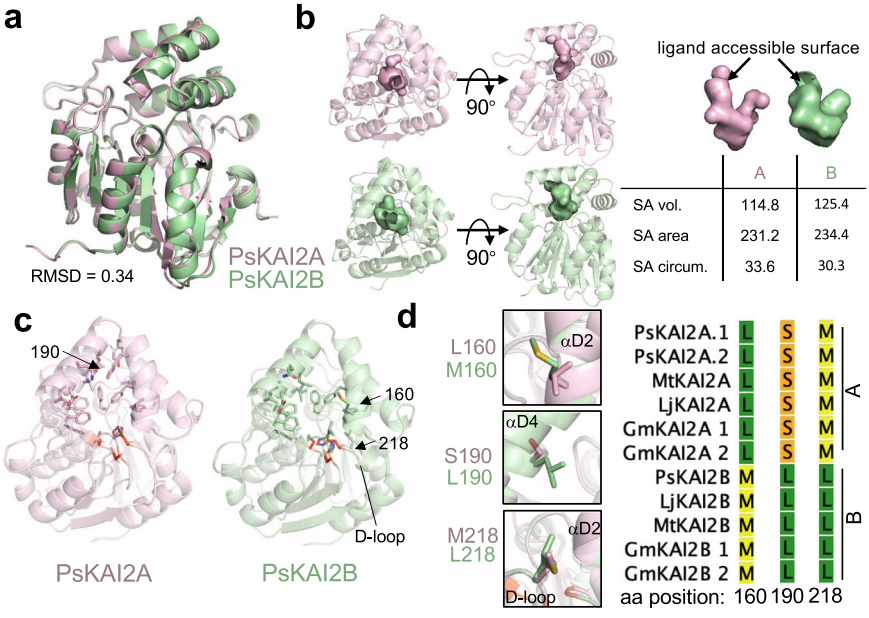

Fig. 7 Structural divergence analysis of legume KAI2A and KAI2B. a Structural alignment of PsKAI2A and PsKAI2B shown in pink and light green colors respectively. RMSD of aligned structures is shown. **b** Analysis of PsKAI2A and PsKAI2B pocket volume, area, and morphology is shown by solvent accessible surface presentation. Pocket size values were calculated via the CASTp server. **c** Residues involved in defining ligand-binding pocket are shown on each structure as sticks. Catalytic triad is shown in red. **d** Residues L/M160, S/L190, and M/L218 are highlighted as divergent legume KAI2 residues, conserved among all legume KAI2A or KAI2B sequences as shown in reduced Multiple Sequence Alignment from Supplementary Fig. 3.

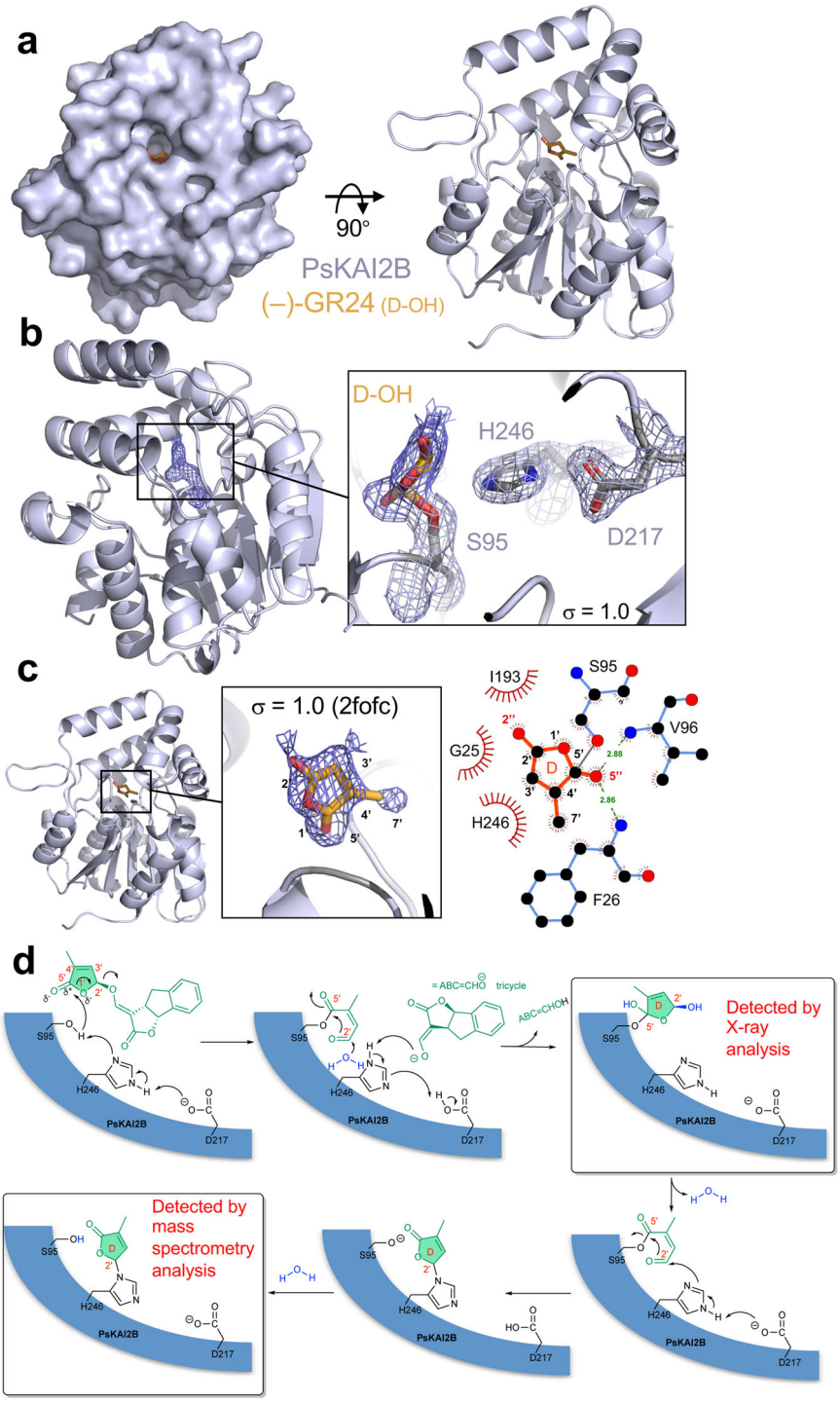

Fig. 8 Structural basis of PsKAI2B ligand interaction. a Surface (left) and cartoon (right) representations of PsKAI2B crystal structure in complex with (–)-GR24 D-OH ring. Protein structure is shown in blue/gray and ligand in orange. **b** Close-up view on ligand interactions and contiguous density with the catalytic serine S95. Electron density for the ligand is shown in navy blue and blue/gray mesh for the labeled catalytic triad. The contiguous density between S95 and the D-OH ring indicates a covalent bond. The electron density is derived from 2mFoDFc (2fofc) map contoured at 1.0 s. **c** Side view of PsKAI2B-D-OH structure shown in cartoon with highlighted (orange) the intact D-OH ring structure. 2-D ligand interaction plot was generated using LigPlot+ software. Dark gray line represents S95-D-OH ring covalent bond. **d** Schematic diagram of the proposed mechanism for the formation of the D-ring intermediate covalently bound to S95 in a first time and then to H246.

I193 residues. Notably, the electron density around the S95 does not display an open D-OH group (2,4,4,-trihydroxy-3-methyl-3-butenal as previously described for OsD14[21]) that could directly result from the nucleophilic attack event, but rather more closely corresponds to a cyclized D-OH ring linked to the S95. The D-OH ring is likely to be formed by water addition to the carbonyl group at C2' that is generated after cleavage of the enol function and cyclization to re-form the butenolide (Fig. 8d). Based on the suggested mechanism of SL hydrolysis by D14[36,50,52,55], we propose that the formation of the S95-adduct

serves as a highly transient intermediate before its transfer to the catalytic histidine residue. Therefore, to further examine (–)-GR24 catalysis by PsKAI2s, we recorded mass spectrometry (MS) spectra under denaturing conditions with PsKAI2B and PsKAI2A. As expected, a mass shift occurred corresponding to an intermediate covalently bound to PsKAI2s (Supplementary Fig. 13a-d). Following digestion, a peptide with additional mass of 96 Da was detected on the catalytic residue H246, further corroborating the transient nature of S95-adduct that was captured in the crystal structure (Supplementary Fig. 13e-f). Collectively, the crystal structure of PsKAI2B bound to GR24 and the MS data show transient and stable intermediates attached to S95 and H246 of the catalytic triad and reveal the mode of action of KAI2 as receptors and enzymes (Fig. 8d).

Discussion

The coevolution between receptors and ligands in diverse environments throughout plant evolution is of wide interest in many biological fields. In particular, characterization of the emerging karrikin/KL signaling in non-fire following plants has been of increasing importance in plant signaling at large. While there are many missing pieces in the karrikin/KL signaling puzzle, it is clear that KAI2 is the key sensor in this pathway(s). The striking evolutionary conservation of KAI2 receptors in all land plants is not fully explained by the limited natural occurrence of smoke-derived karrikin molecules as well as non-fire following species. Also, an increasing number of studies shows that the functions of KAI2s are preserved to regulate plant development and response to stresses by perceiving KL signals from either internal or external sources. While for D14, the dual function as receptor and enzyme with respect to the exact hydrolysis and perception mechanism is well described, it remains to be characterized for KAI2. Here, we identified and characterized the KAI2 receptors in pea (*P. sativum*) that serve as representatives to examine KAI2 sub-functionalization in legumes. The identification of both *PsKAI2A* and *PsKAI2B* genes corroborates the recent finding that the *KAI2* gene duplication event occurred in Papilionoidaea before the diversification of legumes[38]. The similarities in gene expression patterns are found between pea and *Lotus* with globally higher expression of *KAI2A* in comparison to *KAI2B* and higher expression *KAI2B* versus *KAI2A* in roots, depending on whether the plants are grown in pots or Petri dishes. PsKAI2 TILLING mutant lines did not show significant branching and root hair phenotypes. Future studies of pea *Pskai2a/b* mutants will further elucidate the distinct physiological functions, in particularly their symbiotic relationship with AM fungi and the differential expression patterns in the roots. Interestingly, both pea single mutants can induce the expression of *PsDLK2* in response to (–)-GR24, which is in agreement with the observation that *L. japonicus* KAI2B cannot bind (–)-GR24[38] due to the hindering W158, which is absent from pea PsKAI2s. Furthermore, our DSF analyses confirms that PsKAI2B differs from its ortholog in *L. japonicus*, which is not destabilized by (–)-GR24 due to the rare phenylalanine to tryptophan exchange at position 158 at the binding pocket[38]. The Arabidopsis complementation experiments with pea KAI2s verified the distinct functionalities of PsKAI2A and PsKAI2B, wherein PsKAI2A most closely resembles AtKAI2 complementation in hypocotyl elongation assays indicating sensitivity to the endogenous KL, while PsKAI2B and not PsKAI2A is able to rescue the sensitivity of the *htl-3* and *kai2-2* mutants to (–)-GR24.

Molecular coevolution of ligands and their specialized receptors has been previously demonstrated for phytohormones such as SL[56], ABA[57], GA[58], and more recently, karrikins[35,38]. The diversification of KAI2 receptors in different species suggests a diversification of ligands. Interestingly, the SL receptor D14 usually occurs as a single copy gene, although strigolactones are strongly diversified. It will be intriguing to reveal whether this means that KLs are even more structurally diverse than SLs, or whether the SL diversity reflects more strongly their functions in the rhizosphere than their hormonal functions in planta, which can also be fulfilled by carlactone[59]. Indeed, the *true* nature of the branching inhibitor is still under discussion and remains to be fully resolved as suggested by the non-branching phenotype of the SL deficient tomato *cyp722c* and lotus *Ljmax1* mutants[60–62]. Even though the exact identity of KL remains to be revealed, it is thought that the ligands likely share structural commonalities with SLs. As such, it has been recently shown that one enantiomer of the artificial SL analog, *rac*-GR24, can function by binding KAI2 in Arabidopsis[9,39,51]. Here we show that PsKAI2B can form stronger interactions with the enantiomer (–)-GR24, compared to PsKAI2A. Moreover, we found that while both KAI2s are active hydrolases, they have distinct binding affinity and stereoselectivity towards GR24 stereoisomers. These findings indicate that sub-functionalization of KAI2s via substitutions in only few amino acids can greatly alter ligand affinity, binding, enzymatic activity, and probably signaling with downstream partners[34,38].

To better elucidate the molecular divergence of PsKAI2A and B and their dual receptor-enzyme function, we carried out extensive biochemical and structural studies. KAI2/D14 crystal structures have greatly impacted our understanding of their ligand-binding pockets and their ability to not only accommodate, but also hydrolyze certain ligands[9,21,32,34,40–42]. The crystal structure of PsKAI2B together with the PsKAI2A homology model reported here, further substantiates the structural basis of this differential ligand selectivity. We identified conserved key amino acid changes that alter the shape of the pocket and confer altered ligand specificities. These atomic structures of legume KAI2 enabled us to analyze the distinction between key residues L160/S190/M218 in PsKAI2A and the corresponding residues M160/L190/L218 in PsKAI2B. Further swap experiments between residues 160 and 190 confirmed that these residues are necessary for the sensitivity of PsKAI2B for (–)-GR24, but not sufficient to bring PsKAI2A to similar sensitivities. These findings support recent *in planta* studies that demonstrate that residues 160 and 190 are required for differential ligand specificity between *Lotus* KAI2A and KAI2B[38]. Furthermore, the residue in position 190 was also identified in the parasitic plant *Striga hermonthica* as being involved in determining specificity of divergent pockets between the highly variable and functionally distinct HTLs[31,32]. While the changes in positions 160 and 190 directly reshape the pocket morphology, the variant in position 218 is located in the center of the D-loop that has been suggested in downstream protein-protein interactions in SL signaling[54,55]. Therefore, the conserved substitution of KAI2A and KAI2B in M218 to L218 respectively across legumes may also contribute to downstream interaction(s), of which remains to be elucidated. Based on the analogy with the D14-MAX2 perception mechanism, the KAI2 receptor is likely to adopt different conformational states upon ligand binding and cleavage. As such, the identification of unique residue variations in the lid (between KAI2A and KAI2B, respectively in positions 129 and 147) as well as the D-loop (position 218) reported here, infer a sub-functionalization in the receptor regions that are likely to be involved in MAX2 and/or SMAX1 and/or SMXL2 downstream interactions. Therefore, it remains to be further elucidated whether these distinctive residues play a role in fine tuning the formation of the protein complex with MAX2-SMAX1/SMXL2.

The crystal structure of ligand-bound PsKAI2B provides a unique mechanistic view of perception and cleavage by KAI2s. Based on the crystallization conditions and following a detailed

investigation of the electron density, we were able to overrule common chemicals and place the (–)-GR24 D-OH ring with higher relative fitting values than other components. The absence of positive electron density peaks corresponding to the intact (–)-GR24, and thus the presence of only the D-OH ring, raise questions of whether the S95-D-OH adduct recapitulates a pre- or post- cleavage intermediate state of (–)-GR24. The possibility that the trapped molecule represents a post cleavage state is intriguing and may provide a new intermediate state where S95 is covalently linked to the cleavage product. As such, the S95-D-OH adduct suggested here could explain the single turnover cycle that was observed for KAI2s in this study. This could be further corroborated by evidence in Arabidopsis that KAI2s are often degraded post-hydrolysis of their ligand, suggesting that KAI2 acts as a single turnover enzyme, degrading its signal and then itself[63]. While early structural studies of D14 hydrolysis also positioned the catalytic serine with a covalent adduct[21], other studies of the single turnover activity of D14 suggest that a covalent intermediate is in fact formed between the catalytic histidine and serine[55]. The chemical similarity of the D-OH butenolide ring of karrikin and GR24 suggests that the KL signal may share a parallel structure and perhaps is biochemically processed via multiple steps and intermediate adducts. Therefore, the significance of this finding may also shed light on SL perception and cleavage by D14, which are still elusive. While the MS data corroborate a mass shift corresponding to an intermediate covalently bound to KAI2s, the adduct was detected more significantly on the catalytic histidine rather than on the serine. This data is in agreement with the expected transient nature of the serine nucleophilic attack, and the more stable adduct that can be formed on the catalytic histidine. Collectively, the crystal structure of PsKAI2B bound to enantiomeric SL synthetic analog and the MS data reveal the mode of action of KAI2 not only as receptors but also as bona fide enzymes. Beyond the importance of illuminating the stereoselectivity of ligand perception and cleavage diverged KAI2 receptors in KAR/KL signaling pathways, our data strongly suggest that through the evolution of KAI2 enzymes, specific structural and functional adaptation diverged to enable more extended sensitivities to KAR/KL and SL and SL-like molecules by KAI2B.

Here, we elucidate the molecular basis for functional divergence of KAI2 receptors, focusing on pea as model legume. Because of their ability to fix atmospheric nitrogen through plant–rhizobium symbiosis, legume crops such as pea or fava bean are attracting increasing attention for their agroecological potential. Thus, better understanding of KAR/KL perception, hydrolysis mechanisms, and signaling in these key crops may have far-reaching impacts on agro-systems and food security.

Methods

Protein sequence alignment and phylogenetic tree analyses. Representative KAI2 sequences of 41 amino acid sequences were downloaded from Phytozome and specific genome databases as shown in Supplementary Fig. 1. Alignment was performed in MEGA X[64] using the MUSCLE multiple sequence alignment algorithm[65]. Sequence alignment graphics were generated using CLC Genomics Workbench v12. The evolutionary history was inferred by using the Maximum Likelihood method and JTT matrix-based model[66]. Initial tree(s) for the heuristic search were obtained automatically by applying Neighbor-Join and BioNJ algorithms to a matrix of pairwise distances estimated using the JTT model, and then selecting the topology with superior log likelihood value. The percentage of trees in which the associated taxa clustered together is shown next to the branches[67]. Tree is drawn to scale, with branch lengths measured in the number of substitutions per site. Analysis involved 41 amino acid sequences with a total of 327 positions in the final dataset. Evolutionary analyses were conducted in MEGA X[64].

RT-PCR analyses. For PsKAI2A splicing variant detection, PCR reactions were performed using 1 µl of cDNA or genomic DNA sample in a final reaction mixture (20 µl) containing 2 µl of 10 x PCR buffer (ThermoFisher Scientific), 0.25 µL of 25 mM dNTPs, 0.25 µl of each primer at 10 µM, and 1 unit of Dream Taq DNA polymerase (ThermoFisher Scientific). Primer sequences are indicated in Supplementary Table 2. PCR was performed in the following conditions: 94 °C/ 5 min, 94 °C/30 s, 58 °C/30 s, 72 °C/1 min for 30 cycles. Half of each PCR product was loaded onto Ethidium bromide stained 1% agarose gels in TAE buffer, stained with ethidium bromide, and photographed with Molecular Imager® Gel Doc™ XR System (BioRad)

Constructs and generation of transgenic lines. The expression vectors for transgenic Arabidopsis were constructed by MultiSite Gateway Three-Fragment Vector Construction kit (Invitrogen). *AtKAI2* and *PsKAI2A.2* constructs were tagged with 6xHA epitope tag, mCitrine protein or GUS protein at their C-terminus. Lines were resistant to hygromycin. The *AtKAI2* native promoter (0.7 kb) was cloned into the pDONR-P4P1R vector, using Gateway recombination (Invitrogen) as described in[68]. The 6xHA with linker and mCitrine tags were cloned into pDONR-P2RP3 (Invitrogen) as described in de Saint Germain et al. [50]. *PsKAI2A.1*, *PsKAI2A.2* and *PsKAI2B* CDS were PCR amplified from *Pisum* cv. Térèse cDNA with the primers specified in Supplementary Table 2 and then recombined into the pDONR221 vector (Invitrogen). The suitable combination of *AtKAI2* native promoter, *AtKAI2*, *PsKAI2A.1*, *PsKAI2A.2* or *PsKAI2B* and 6XHA,mCitrine or GUS was cloned into the pH7m34GW final destination vectors by using the three fragment recombination system[69] and were thusly named proAtKAI2:AtKAI2-6xHA, proAtKAI2:AtKAI2-mcitrine, proAtKAI2:AtKAI2-GUS, proAtKAI2:PsKAI2A.1-6xHA, proAtKAI2:PsKAI2A.2-mcitrine, proAtKAI2:PsKAI2A.2-GUS, proAtKAI2:PsKAI2B-6XHA, proAtKAI2:PsKAI2B-GUS and proAtKAI2:PsKAI2B-mcitrine. Transformation of Arabidopsis *htl-3* or *kai2-2* mutant was performed according to the conventional floral dipping method[70], with Agrobacterium strain GV3101. For each construct, only a few independent T1 lines were isolated, and all lines were selected in T2. Phenotypic analysis shown in Fig. 3 and Supplementary Fig. 5-6 were performed on the T3 homozygous lines.

Protein extraction and immunoblotting. Total protein extract was prepared from $n = 8$ to $n = 10$, 10 day-old Arabidopsis seedlings in Laemmli buffer and boiled for 5 min. Total protein were separated by 10% SDS-PAGE and transferred onto polyvinylidene difluoride membrane (Bio-Rad) probed with anti-HA primary antibody (1:10000; SIGMA H9658-100UL Lot#128M4789V) and then anti-mouse-IgG-HRP secondary antibody (1:10000; SIGMA A9044-2ML-100UL Lot#029M4799V) or with anti-GFP primary antibody (1:10000; CHROMTEK 3H9-100 Lot#60706001AB) and then anti-rat-IgG-HRP secondary antibody (1:10000; SIGMA A9037-1ML Lot#SLCF6775). Ponceau staining was used as a loading control.

Identification of Pskai2a and Pskai2b targeting-induced local lesions IN genomes (TILLING) mutants. The mutagenized population in the pea cultivar (cv.) Caméor was used as a TILLING resource. For obtaining mutants in *PsKAI2A*, TILLING analysis was performed on 5000 families within one amplicon of 1068 bp using nested primers (N1, N2) with PsKAI2A_N1F primer and PsKAI2A_N1R primer PsKAI2A_N2Ftag primer and PsKAI2A_N2Rtag primer Primers are indicated in Supplementary Table 2. The enzymatic mutation detection technique based on the mismatch specific endonuclease ENDO1 was used. For *PsKAI2B*, the mutation detection system by sequencing and described in[71] was used. Two amplicons of 381 and 401 bp were screened in 2500 families. Primers are indicated in Supplementary Table 2. Prediction of the amino acid changes that affect protein function was made using the SIFT program (sift.jcvi.org/).

M3 and M4 seeds from lines carrying mutations in the *PsKAI2A* and *PsKAI2B* genes were genotyped for homozygous mutant plants; these plants were backcrossed once (alleles *Pskai2a-4, Pskai2b-1, Pskai2b-2*) to three or four times (alleles *Pskai2a-2, Pskai2a-6, Pskai2b-3*) to the cv. Caméor. BC1-F3 and M5 single mutant plants were crossed for obtaining the *Pskai2a-6 Pskai2b-3* double mutant.

Plant material and growth conditions. For branching quantification, *Pisum sativum* plants were grown in glasshouse (23 °C day/ 15 °C night) under a 16-h photoperiod (the natural daylength was extended or supplemented during the day when necessary using sodium lamps) in pots filled with clay pellets, peat, and soil (1:1:1) supplied regularly with nutrient solution. Nodes were numbered acropetally from the first scale leaf as node 1.

Root hair assay. *Pisum sativum Cameor* wild-type, *Pskai2a-3*, *Pskai2b-6*, *Pskai2a-3 Pskai2a-6* seeds were surface sterilized with 1% NaClO, washed 5 times, and incubated for 2 h in sterile water. Imbibed seeds were germinated on ½ MS, pH 5.8 containing 1% agar at 4 °C for 3 days in the dark. Seedlings were grown in axenic conditions on 12 × 12 cm square Petri dishes at 24 °C with 16-h-light/8-h-dark cycles. To assess root hair length, images of the primary root tips of 10-day old seedlings were taken with a Zeiss Discovery V8 microscope equipped with a Zeiss Axiocam 503 camera. Root hair length was measured for a minimum of 8 roots per genotype for 8 different root hairs per root, between 10 and 20 mm from the root tip using Fiji as described[72]. For root-hair length measurements a Welch t test, p value < 0.05 and for RT-qPCR analysis a Kruskal-Wallis Test with post-hoc Student's t test, $p < 0.05$ were performed using R statistical environment (https://www.r-project.org/). For the Kruskal-Wallis Test the R-package agricolae (https://CRAN.R-project.org/package=agricolae) was used.

Treatment for analysis of transcript accumulation. For treatments with KARs and GR24 enantiomers, 10-day old seedlings grown on Petri dishes as described above, were placed with their roots into 50 ml amber Falcon tubes filled with ½ MS solution for 24 h to allow the seedlings to adapt to the new growth system. For the treatment the growth media was exchanged with ½ MS solution containing 3 µM Karrikin$_1$, Karrikin$_2$, (www.olchemim.cz), (+)-GR24 or (–)-GR24 (www.strigolab.eu) and seedlings were incubated with their shoots in the light for 4 h.

Analysis of transcript accumulation by RT-qPCR. For analysis of transcript levels by RT-qPCR presented in Fig. 1, total RNA was isolated from 28 days old plant for flower and flower bud and from 10 days old plants for all other tissues, using TRIZOL reagent (Invitrogen) following the manufacturer's protocol. DNase treatment was performed to remove DNA using the Qiagen RNase-Free DNase Set (79254) and the RNeasy Mini Kit (74904) and eluted in 50 mL of RNase-free water. RNA was quantified using NanoDrop 1000 and migrated on gels to check RNA non-degradation. Total cDNA was synthesized from 2 mg of total RNA using 50 units of RevertAid H Moloney murine leukemia virus reverse transcriptase in 30 µL following the manufacturer's instructions with poly(T)18 primer. cDNA was diluted 10 times before subsequent analysis. Quantitative reverse transcription-PCR analyses were adapted from[73]. They were performed using SsoAdvancedTM Universal SYBR® Green SuperMix (Biorad). Cycling conditions for amplification were 95 °C for 10 min, 50 cycles of 95 °C for 5 s, 62 °C for 5 s, and 72 °C for 15 s, followed by 0.1 °C s–1 ramping up to 95 °C for fusion curve characterization. Two biological repeats were analyzed in duplicate. To calculate relative transcript levels, the comparative cycle method based on non-equal efficiencies was used[74]. Transcript levels for the different genes were expressed relative to the expression of the *PsACTIN* gene. Primers are indicated in Supplementary Table 2.

For analysis of transcript levels by RT-qPCR presented in Fig. 2, plant tissue was rapidly shock frozen in liquid nitrogen and ground to a fine powder with a mortar and pestle. RNA was extracted using the Spectrum Plant Total RNA Kit (www.sigmaaldrich.com). The RNA was treated with Invitrogen DNAse I amp. grade (www.invitrogen.com) and tested for purity by PCR. cDNA synthesis was performed with 1 µg RNA using the iScript cDNA Synthesis kit (www.Biorad.com). cDNA was diluted in water in a 1:10 ratio and 1 µl was used for RT-PCR was performed with an iCycler (Biorad, www.bio-rad.com/) using a Green MasterMix (Jena Bioscience, highROX, 2x conc.). Thermal cycler conditions were: 95 °C 2 min, 45 cycles of 95 °C 30 sec, 60 °C 30 sec and 72 °C 20 sec followed by dissociation curve analysis. Expression levels were calculated according to the ΔΔCt method[75]. For each genotype and treatment three to four biological replicates were monitored and each sample was represented by two technical replicates. Transcript levels for the different genes were expressed relative to the expression of the *PsTUB* gene, Accession:X54844[76]. Primers are indicated in Supplementary Table 2.

Hypocotyl elongation assays. Arabidopsis seeds were surface sterilized by consecutive treatments of 5 min 70% (v/v) ethanol with 0.05% (w/v) sodium dodecyl sulfate (SDS) and 5 min 95% (v/v) ethanol. Then seeds were sown on half-strength Murashige and Skoog (½ MS) media (Duchefa Biochemie) containing 1% agar, supplemented with 1 µM (–)-GR24 or with 0.01 % DMSO (control). Seeds were stratified at 4 °C (2 days in dark) then transferred to the growth chamber at 22 °C, under 20-30 µE /m^2/sec of white light in long day conditions (16 hr light/ 8 hr dark). Seedlings were photographed and hypocotyl lengths were quantified using ImageJ[77]. 2 plates of 10-12 seeds were sown for each genotype x treatment. Using Student *t* tests, no statistically significantly different means were detected between plates. The data from the 20 to 24 seedlings were then used for a one-way ANOVA.

Chemicals. Enantiopure GR24 isomers were obtained as described in de Saint Germain et al. [50] or purchased from StrigoLab. Karrikin$_1$ and Karrikin$_2$ were purchased from Olchemim. Profluorescent probes (GC240, GC486) were obtained as described in de Saint Germain et al. [50,78].

Protein preparation and purification. PsKAI2A.2, PsKAI2B, and all described mutants were independently cloned and expressed as a 6× His-SUMO fusion proteins from the expression vector pAL (Addgene). These were cloned utilizing primers in Supplementary Table 2. BL21 (DE3) cells transformed with the expression plasmid were grown in LB broth at 16 °C to an OD$_{600}$ of ~0.8 and induced with 0.2 mM IPTG for 16 h. Cells were harvested, re-suspended and lysed in extract buffer (50 mM Tris, pH 8.0, 200 mM NaCl, 5 mM imidazole, 4% Glycerol). All His-SUMO-PsKAI2s were isolated from soluble cell lysate by Ni-NTA resin. The His-SUMO-PsKAI2 was eluted with 250 mM imidazole and subjected to anion-exchange. The eluted protein was than cleaved with TEV (tobacco etch virus) protease overnight at 4 °C. The cleaved His-SUMO tag was removed by passing through a Nickel Sepharose and PsKAI2 was further purified by chromatography through a Superdex-200 gel filtration column in 20 mM HEPES, pH 7.2, 150 mM NaCl, 5 mM DTT, 1% Glycerol. All proteins were concentrated by ultrafiltration to 3–10 mg/mL^{-1}. RMS3, AtD14, AtKAI2 were expressed in bacteria with TEV cleavable GST tag, purified and used as described in de Saint Germain et al. [50].

Enzymatic hydrolysis of GR24 isomers by purified proteins. Ligands (10 µM) were incubated without and with purified proteins (5 µM) for 150 min at 25 °C in PBS (0.1 mL, pH 6.8) in presence of (±)-1-indanol (100 µM) as the internal standard. The solutions were acidified to pH 1 with 10% trifluoroacetic acid in CH_3CN (v/v) (2 µL) to quench the reaction and centrifuged (12 min, 12,000 tr/min). Thereafter the samples were subjected to RP-UPLC-MS analyses using Ultra Performance Liquid Chromatography system equipped with a PDA and a Triple Quadrupole mass spectrometer Detector (Acquity UPLC-TQD, Waters, USA). RP-UPLC (HSS C_{18} column, 1.8 µm, 2.1 mm × 50 mm) with 0.1% formic acid in CH_3CN and 0.1% formic acid in water (aq. FA, 0.1%, v/v, pH 2.8) as eluents [10% CH_3CN, followed by linear gradient from 10 to 100% of CH_3CN (4 min)] was carried out at a flow rate of 0.6 mL/min. The detection was performed by PDA using the TQD mass spectrometer operated in Electrospray ionization positive mode at 3.2 kV capillary voltage. The cone voltage and collision energy were optimized to maximize the signal and were respectively 20 V for cone voltage and 12 eV for collision energy and the collision gas used was argon at a pressure maintained near $4.5.10^{-3}$ mBar.

Enzymatic assay with pro-fluorescent probes. Enzymatic assay and analysis have been carried out as described in de Saint Germain et al. [50], using a TriStar LB 941 Multimode Microplate Reader from Berthold Technologies. The experiments were repeated three times.

Protein melting temperatures. Differential Scanning Fluorimetry (DSF) experiments were performed on a CFX96 TouchTM Real-Time PCR Detection System (Bio-Rad Laboratories, Inc., Hercules, California, USA) using excitation and emission wavelengths of 490 and 575 nm, respectively. Sypro Orange ($\lambda_{ex}/\lambda_{em}$: 470/570 nm; Life Technologies Co., Carlsbad, California, USA) was used as the reporter dye. Samples were heat-denatured using a linear 25 to 95 °C gradient at a rate of 1.3 °C per minute after incubation at 25 °C for 30 min in the absence of light. The denaturation curve was obtained using CFX manager™ software. Final reaction mixtures were prepared in triplicate in 96-well white microplates, and each reaction was carried out in 20 µL scale in Phosphate buffer saline (PBS) (100 mM Phosphate, pH 6.8, 150 mM NaCl) containing 6 µg protein (such that final reactions contained 10 µM protein), 0-1000 µM ligand (as shown on the Fig. 4c–f and Supplementary Fig. 8,11), 4% (v/v) DMSO, and 0.008 µL Sypro Orange. Plates were incubated in darkness for 30 min before analysis. In the control reaction, DMSO was added instead of ligand. All experiments were repeated three times.

Intrinsic tryptophan fluorescence assays and kinetics. Intrinsic tryptophan fluorescence assays and determination of the dissociation constant K_D has been performed as described in de Saint Germain et al. [50], using the Spark® Multimode Microplate Reader from Tecan.

Crystallization, data collection and structure determination. The crystals of PsKAI2B were grown at 25 °C by the hanging-drop vapor diffusion method with 1.0 µL purified protein sample mixed with an equal volume of reservoir solution containing 0.1 M HEPES pH 7.5, 2.75% PEG 2000, 2.75% v/v PEG 3350, 2.75% v/v PEG 4000, 2.75% v/v PEG-ME 5000. The crystals of PsKAI2B in complex with (–)-GR24 were grown at 25 °C by the hanging-drop vapor diffusion method with 1.0 µL purified protein complex (preincubated with 1 mM (–)-GR24, StrigoLab) and mixed with an equal volume of reservoir solution containing 0.1 M HEPES pH 7.5, 2.75% PEG 2000, 2.75% v/v PEG 3350, 2.75% V/V PEG 4000, 2.75% v/v PEG-ME 5000, 1 mM (–)-GR24. Crystals of maximum size were obtained and harvested after 2 weeks from the reservoir solution with additional 20% MPD serving as cryoprotectant. X-ray diffraction data was integrated and scaled with HKL2000 package[79]. PsKAI2s crystal structures were determined by molecular replacement using the AtKAI2 model (PDB: 5Z9H)[80] as the search model. All structural models were manually built, refined, and rebuilt with PHENIX[81] and COOT[82].

Structural biology modeling and analyses. Model structure illustrations were made by PyMOL[83]. PsKAI2A model structure was generated using iTASSER[84]. Ligand identification, ligand-binding pocket analyses, and computing solvent accessible surface values analyses were carried out using Phenix LigandFit[81], CASTp software[85], and AutoDock Vina[86], respectively. LigPlot+ program[87] was used for 2-D representation of protein-ligand interactions from standard PDB data format.

Direct electrospray ionization – mass spectrometry of PsKAI2 proteins (ESI)-MS under denaturing conditions. Mass spectrometry measurements were performed with an electrospray Q-TOF mass spectrometer (Waters) equipped with the Nanomate device (Advion, Inc.). The HD_A_384 chip (5 µm I.D. nozzle chip, flow rate range 100−500 nL/min) was calibrated before use. For ESI − MS measurements, the Q-TOF instrument was operated in RF quadrupole mode with the TOF data being collected between m/z 400 and 2990. Collision energy was set to 10 eV and argon was used as the collision gas. PsKAI2 proteins (50 µM) in 50 mM ammonium acetate (pH 6.8) in presence or without (-)-GR24 (500 µM) were incubated for 10 min at room temperature before denaturation in 50% acetonitrile and 1% formic acid. The solutions were directly injected for Mass spectra acquisition or digested before LC-MS/MS analyses. Mass Lynx version 4.1 (Waters) and Peakview version 2.2 (Sciex) software were used for acquisition and data

processing, respectively. Deconvolution of multiply charged ions was performed by applying the MaxEnt algorithm (Sciex). The average protein masses were annotated in the spectra and the estimated mass accuracy was ± 2 Da. External calibration was performed with NaI clusters (2 µg/µL, isopropanol/H_2O 50/50, Waters) in the acquisition m/z mass range.

Statistics and reproducibility. Statistical analysis were carried out in R[88]. Unless otherwise indicated, statistical significance of the data was assessed using the non-parametric Kruskal-Wallis rank sum test ($*P < 0.05$) using the nparcomp package or one-way ANOVA with a Tukey multiple comparison of means post-hoc test (lowercase letters: $P < 0.05$).

Reporting summary. Further information on research design is available in the Nature Research Reporting Summary linked to this article.

Data availability

The atomic coordinates of apo and ligand-bound forms of PsKAI2 structures has been deposited in the Protein Data Bank with accession codes 7K2Z and 7K38, respectively. All source data for Figs. 1–6, 8, and Supplementary Fig. 5-6, 8-9, 11 are available in Supplementary Data 1. Any other relevant data are available from corresponding authors upon request.

Received: 9 November 2021; Accepted: 28 January 2022;
Published online: 11 February 2022

References

1. Flematti, G. R., Ghisalberti, E. L., Dixon, K. W. & Trengove, R. D. A compound from smoke that promotes seed germination. *Science* **305**, 977 (2004).
2. Flematti, G. R. et al. Preparation of 2H-furo[2,3-c]pyran-2-one derivatives and evaluation of their germination-promoting activity. *J. Agric. Food Chem.* **55**, 2189–2194 (2007).
3. Flematti, G. R., Scaffidi, A., Dixon, K. W., Smith, S. M. & Ghisalberti, E. L. Production of the seed germination stimulant karrikinolide from combustion of simple carbohydrates. *J. Agric. Food Chem.* **59**, 1195–1198 (2011).
4. Dixon, K. W., Merritt, D. J., Flematti, G. R. & Ghisalberti, E. L. Karrikinolide—A phytoreactive compound derived from smoke with applications in horticulture, ecological restoration and agriculture. *Acta Hortic.* **813**, 155–170 (2009).
5. Stevens, J. C., Merritt, D. J., Flematti, G. R., Ghisalberti, E. L. & Dixon, K. W. Seed germination of agricultural weeds is promoted by the butenolide 3-methyl-2H-furo[2,3-c]pyran-2-one under laboratory and field conditions. *Plant Soil* **298**, 113–124 (2007).
6. Long, R. L. et al. Prior hydration of Brassica tournefortii seeds reduces the stimulatory effect of karrikinolide on germination and increases seed sensitivity to abscisic acid. *Ann. Bot.* **105**, 1063–1070 (2010).
7. Nelson, D. C. et al. F-box protein MAX2 has dual roles in karrikin and strigolactone signaling in Arabidopsis thaliana. *Proc. Natl. Acad. Sci.* **108**, 8897–8902 (2011).
8. Waters, M. T. et al. Specialisation within the DWARF14 protein family confers distinct responses to karrikins and strigolactones in Arabidopsis. *Development* **139**, 1285–1295 (2012).
9. Guo, Y., Zheng, Z., La Clair, J. J., Chory, J. & Noel, J. P. Smoke-derived karrikin perception by the a/B hydrolase KAI2 from Arabidopsis. *Proc. Natl. Acad. Sci.* **110**, 8284–8289 (2013).
10. Kagiyama, M. et al. Structures of D14 and D14L in the strigolactone and karrikin signaling pathways. *Genes Cells* **18**, 147–160 (2013).
11. Stanga, J. P., Smith, S. M., Briggs, W. R. & Nelson, D. C. Suppressor of more axillary GROWTH2 1 controls seed germination and seedling development in Arabidopsis. *Plant Physiol.* **163**, 318–330 (2013).
12. Nelson, D. C. et al. Karrikins enhance light responses during germination and seedling development in Arabidopsis thaliana. *Proc. Natl. Acad. Sci. USA.* **107**, 7095–7100 (2010).
13. Sun, X. D. & Ni, M. HYPOSENSITIVE to LIGHT, an alpha/beta fold protein, acts downstream of ELONGATED HYPOCOTYL 5 to regulate seedling de-etiolation. *Mol. Plant* **4**, 116–126 (2011).
14. Yao, J. & Waters, M. T. Perception of karrikins by plants: A continuing enigma. *J. Exp. Botany* (2020) https://doi.org/10.1093/jxb/erz548.
15. Waters, M. T., Scaffidi, A., Sun, Y. K., Flematti, G. R. & Smith, S. M. The karrikin response system of Arabidopsis. *Plant J.* **79**, 623–631 (2014).
16. Gutjahr, C. et al. Rice perception of symbiotic arbuscular mycorrhizal fungi requires the karrikin receptor complex. *Science* **350**, 1521–1524 (2015).
17. Li, W. et al. The karrikin receptor KAI2 promotes drought resistance in Arabidopsis thaliana. *PLoS Genet.* **13**, e1007076 (2017).
18. Wang, L., Waters, M. T. & Smith, S. M. Karrikin-KAI2 signalling provides Arabidopsis seeds with tolerance to abiotic stress and inhibits germination under conditions unfavourable to seedling establishment. *N. Phytol.* **219**, 605–618 (2018).
19. Scaffidi, A. et al. Exploring the molecular mechanism of karrikins and strigolactones. *Bioorg. Med. Chem. Lett.* **22**, 3743–3746 (2012).
20. Yoneyama, K. Recent progress in the chemistry and biochemistry of strigolactones. *J. Pestic. Sci.* **45**, 45–53 (2020).
21. Zhao, L. H. et al. Crystal structures of two phytohormone signal-transducing α/β hydrolases: Karrikin-signaling KAI2 and strigolactone-signaling DWARF14. *Cell Res.* **23**, 436–439 (2013).
22. Akiyama, K., Matsuzaki, K. I. & Hayashi, H. Plant sesquiterpenes induce hyphal branching in arbuscular mycorrhizal fungi. *Nature* **435**, 824–827 (2005).
23. Gomez-Roldan, V. et al. Strigolactone inhibition of shoot branching. *Nature* **455**, 189–194 (2008).
24. Agusti, J. et al. Strigolactone signaling is required for auxin-dependent stimulation of secondary growth in plants. *Proc. Natl Acad. Sci. USA* **180**, 20242–20247 (2011).
25. Kapulnik, Y. et al. Strigolactones affect lateral root formation and root-hair elongation in Arabidopsis. *Planta* **233**, 209–216 (2011).
26. Rasmussen, A. et al. Strigolactones suppress adventitious rooting in arabidopsis and pea. *Plant Physiol.* **158**, 1976–1987 (2012).
27. Waters, M. T., Gutjahr, C., Bennett, T. & Nelson, D. C. Strigolactone signaling and evolution. *Annu. Rev. Plant Biol.* **68**, 291–322 (2017).
28. Cook, C. E., Whichard, L. P., Turner, B., Wall, M. E. & Egley, G. H. Germination of witchweed (striga lutea lour.): Isolation and properties of a potent stimulant. *Science* **154**, 1189–1190 (1966).
29. Bythell-Douglas, R. et al. Evolution of strigolactone receptors by gradual neo-functionalization of KAI2 paralogues. *BMC Biol.* **15**, 1–21 (2017).
30. Swarbreck, S. M., Guerringue, Y., Matthus, E., Jamieson, F. J. C. & Davies, J. M. Impairment in karrikin but not strigolactone sensing enhances root skewing in Arabidopsis thaliana. *Plant J.* **98**, 607–621 (2019).
31. Toh, S. et al. Structure-function analysis identifies highly sensitive strigolactone receptors in Striga. *Science* **350**, 203–207 (2015).
32. Xu, Y. et al. Structural basis of unique ligand specificity of KAI2-like protein from parasitic weed Striga hermonthica. *Sci. Rep.* **6**, 1–9 (2016).
33. Waters, M. T. et al. A selaginella moellendorffii ortholog of KARRIKIN INSENSITIVE2 functions in arabidopsis development but cannot mediate responses to karrikins or strigolactones. *Plant Cell* **27**, 1925–1944 (2015).
34. Bürger, M. et al. Structural Basis of Karrikin and Non-natural Strigolactone Perception in Physcomitrella patens. *Cell Rep.* **26**, 855–865 (2019).
35. Sun, Y. K. et al. Divergent receptor proteins confer responses to different karrikins in two ephemeral weeds. *Nat. Commun.* **11**, (2020). https://doi.org/10.1038/s41467-020-14991-w.
36. de Saint Germain, A. et al. A Phelipanche ramosa KAI2 protein perceives strigolactones and isothiocyanates enzymatically. *Plant Commun.* (2021) https://doi.org/10.1016/j.xplc.2021.100166.
37. Sun, Y. K., Flematti, G. R., Smith, S. M. & Waters, M. T. Reporter gene-facilitated detection of compounds in arabidopsis leaf extracts that activate the karrikin signaling pathway. *Front. Plant Sci.* **7**, 1799 (2016).
38. Carbonnel, S. et al. Lotus japonicus karrikin receptors display divergent ligand-binding specificities and organ-dependent redundancy. *PLoS Genet.* **16**, (2020). https://doi.org/10.1371/journal.pgen.1009249.
39. Conn, C. E. & Nelson, D. C. Evidence that KARRIKIN-INSENSITIVE2 (KAI2) Receptors may Perceive an Unknown Signal that is not Karrikin or Strigolactone. *Front. Plant Sci.* **6**, 1–7 (2016).
40. Hamiaux, C. et al. DAD2 is an α/β hydrolase likely to be involved in the perception of the plant branching hormone, strigolactone. *Curr. Biol.* **22**, 2032–2036 (2012).
41. Zhao, L. H. et al. Destabilization of strigolactone receptor DWARF14 by binding of ligand and E3-ligase signaling effector DWARF3. *Cell Res.* **25**, 1219–1236 (2015).
42. Xu, Y. et al. Structural analysis of HTL and D14 proteins reveals the basis for ligand selectivity in Striga. *Nat. Commun.* **9**, 3947 (2018).
43. Kreplak, J. et al. A reference genome for pea provides insight into legume genome evolution. *Nat. Genet.* **51**, 1411–1422 (2019).
44. Triques, K. *et al.* Characterization of Arabidopsis thaliana mismatch specific endonucleases: Application to mutation discovery by TILLING in pea. *Plant J.* **51**, (2007). https://doi.org/10.1111/j.1365-313X.2007.03201.x.
45. Dalmais, M. *et al.* UTILLdb, a Pisum sativum in silico forward and reverse genetics tool. *Genome Biol.* **9**, (2008). https://doi.org/10.1186/gb-2008-9-2-r43.
46. Villaécija-Aguilar, J. A. et al. SMAX1/SMXL2 regulate root and root hair development downstream of KAI2-mediated signalling in Arabidopsis. *PLoS Genet.* (2019) https://doi.org/10.1371/journal.pgen.1008327.
47. Waters, M. T., Scaffidi, A., Flematti, G. R. & Smith, S. M. The origins and mechanisms of karrikin signalling. *Curr. Opin. Plant Biol.* **16**, 667–673 (2013).
48. Scaffidi, A. et al. Strigolactone hormones and their stereoisomers signal through two related receptor proteins to induce different physiological responses in arabidopsis. *Plant Physiol.* **165**, 1221–1232 (2014).

49. Niesen, F. H., Berglund, H. & Vedadi, M. The use of differential scanning fluorimetry to detect ligand interactions that promote protein stability. *Nat. Protoc.* **2**, (2007). https://doi.org/10.1038/nprot.2007.321.
50. De Saint Germain, A. et al. An histidine covalent receptor and butenolide complex mediates strigolactone perception. *Nat. Chem. Biol.* **12**, 787–794 (2016).
51. Yao, J. et al. An allelic series at the KARRIKIN INSENSITIVE 2 locus of Arabidopsis thaliana decouples ligand hydrolysis and receptor degradation from downstream signalling. *Plant J.* **96**, 75–89 (2018).
52. Yao, R. et al. ShHTL7 is a non-canonical receptor for strigolactones in root parasitic weeds. *Cell Res.* vol. 27 (2017). https://doi.org/10.1038/cr.2017.3.
53. Bythell-Douglas, R. et al. The structure of the Karrikin-Insensitive Protein (KAI2) in Arabidopsis thaliana. *PLoS One* **8**, e54758 (2013).
54. Seto, Y. et al. Strigolactone perception and deactivation by a hydrolase receptor DWARF14. *Nat. Commun.* **10**, 191 (2019).
55. Yao, R. et al. DWARF14 is a non-canonical hormone receptor for strigolactone. *Nature* **536**, 469–473 (2016).
56. Conn, C. E. et al. Convergent evolution of strigolactone perception enabled host detection in parasitic plants. *Science* **349**, 540–543 (2015).
57. Weng, J. K., Ye, M., Li, B. & Noel, J. P. Co-evolution of hormone metabolism and signaling networks expands plant adaptive plasticity. *Cell* **166**, 881–893 (2016).
58. Yoshida, H. et al. Evolution and diversification of the plant gibberellin receptor GID1. *Proc. Natl Acad. Sci. U. S. A.* **115**, E7844–E7853 (2018).
59. Seto, Y. et al. Carlactone is an endogenous biosynthetic precursor for strigolactones. *Proc. Natl. Acad. Sci. USA* **111**, (2014). https://doi.org/10.1073/pnas.1314805111.
60. Yoneyama, K. et al. Which are the major players, canonical or non-canonical strigolactones? *J. Exp. Botany* vol. 69 (2018). https://doi.org/10.1093/jxb/ery090.
61. Wakabayashi, T. et al. Direct conversion of carlactonoic acid to orobanchol by cytochrome P450 CYP722C in strigolactone biosynthesis. *Sci. Adv.* **5**, (2019). https://doi.org/10.1126/sciadv.aax9067.
62. Mori, N. *et al.* Chemical identification of 18-hydroxycarlactonoic acid as an LjMAX1 product and in planta conversion of its methyl ester to canonical and non-canonical strigolactones in Lotus japonicus. *Phytochemistry* **174**, (2020). https://doi.org/10.1016/j.phytochem.2020.112349.
63. Waters, M. T., Scaffidi, A., Flematti, G. & Smith, S. M. Substrate-induced degradation of the α/β-fold hydrolase KARRIKIN INSENSITIVE2 requires a functional catalytic triad but is independent of MAX2. *Mol. Plant* vol. 8 (2015). https://doi.org/10.1016/j.molp.2014.12.020.
64. Kumar, S., Stecher, G., Li, M., Knyaz, C. & Tamura, K. MEGA X: Molecular evolutionary genetics analysis across computing platforms. *Mol. Biol. Evol.* **35**, 1547–1549 (2018).
65. Edgar, R. C. MUSCLE: Multiple sequence alignment with high accuracy and high throughput. *Nucleic Acids Res.* **32**, 1792–1797 (2004).
66. Jones, D. T., Taylor, W. R. & Thornton, J. M. The rapid generation of mutation data matrices from protein sequences. *Bioinformatics* **8**, 275–282 (1992).
67. Felsenstein, J. Confidence Limits on Phylogenies: An Approach Using the Bootstrap. *Evolution (N. Y).* **39**, 783–791 (1985).
68. Lopez-Obando, M. et al. The Physcomitrium (Physcomitrella) patens PpKAI2L receptors for strigolactones and related compounds function via MAX2-dependent and -independent pathways. *Plant Cell* **33**, (2021). https://doi.org/10.1093/plcell/koab217.
69. Karimi, M., Bleys, A., Vanderhaeghen, R. & Hilson, P. Building blocks for plant gene assembly. *Plant Physiol.* **145**, 1183–1191 (2007).
70. Clough, S. J. & Bent, A. F. Floral dip: a simplified method for Agrobacterium-mediated transformation of Arabidopsis thaliana. *Plant J.* **16**, 735–743 (1998).
71. Kirienko, A. N. *et al.* Role of a receptor-like kinase K1 in pea Rhizobium symbiosis development. *Planta* **248**, (2018). https://doi.org/10.1007/s00425-018-2944-4.
72. Villaécija-Aguilar, J. A., Struk, S., Goormachtig, S. & Gutjahr, C. Bioassays for the Effects of Strigolactones and Other Small Molecules on Root and Root Hair Development. in *Strigolactones: Methods and Protocols* (eds. Prandi, C. & Cardinale, F.) 129–142 (Springer US, 2021). https://doi.org/10.1007/978-1-0716-1429-7_11.
73. Braun, N. et al. The pea TCP transcription factor PsBRC1 acts downstream of Strigolactones to control shoot branching. *Plant Physiol.* **158**, 225–238 (2012).
74. Pfaffl, M. W. A new mathematical model for relative quantification in real-time RT-PCR. *Nucleic Acids Res.* **29**, (2001). https://doi.org/10.1093/nar/29.9.e45.
75. Czechowski, T., Bari, R. P., Stitt, M., Scheible, W. R. & Udvardi, M. K. Real-time RT-PCR profiling of over 1400 Arabidopsis transcription factors: Unprecedented sensitivity reveals novel root-and shoot-specific genes. *Plant J.* **38**, (2004). https://doi.org/10.1111/j.1365-313X.2004.02051.x.
76. Knopkiewicz, M. & Wojtaszek, P. Validation of reference genes for gene expression analysis using quantitative polymerase chain reaction in pea lines (Pisum sativum) with different lodging susceptibility. *Ann. Appl. Biol.* **174**, (2019). https://doi.org/10.1111/aab.12475.
77. Schneider, C. A., Rasband, W. S. & Eliceiri, K. W. NIH Image to ImageJ: 25 years of image analysis. *Nat. Methods* **9**, 671–675 (2012).
78. de Saint Germain, A., Clavé, G. & Boyer, F. D. Synthesis of profluorescent strigolactone probes for biochemical studies. in *Methods in Molecular Biology* vol. 2309 (2021).
79. Otwinowski, Z. & Minor, W. Processing of X-ray diffraction data collected in oscillation mode. *Methods Enzymol.* **276**, 307–326 (1997).
80. Lee, I. et al. A missense allele of KARRIKIN-INSENSITIVE2 impairs ligand-binding and downstream signaling in Arabidopsis thaliana. *J. Exp. Bot.* **69**, 3609–3623 (2018).
81. Adams, P. D. et al. PHENIX: A comprehensive Python-based system for macromolecular structure solution. *Acta Crystallogr. Sect. D. Biol. Crystallogr.* **66**, 213–221 (2010).
82. Emsley, P., Lohkamp, B., Scott, W. G. & Cowtan, K. Features and development of Coot. *Acta Crystallogr. Sect. D. Biol. Crystallogr.* **66**, 486–501 (2010).
83. DeLano, W. L. The PyMOL Molecular Graphics System, Version 2.3. *Schrödinger LLC* (2020).
84. Yang, J. & Zhang, Y. I-TASSER server: New development for protein structure and function predictions. *Nucleic Acids Res.* **43**, W174–W181 (2015).
85. Dundas, J. et al. CASTp: Computed atlas of surface topography of proteins with structural and topographical mapping of functionally annotated residues. *Nucleic Acids Res.* **34**, W116–W118 (2006).
86. Steffen, C. et al. AutoDock4 and AutoDockTools4: Automated Docking with Selective Receptor Flexibility. *J. Comput. Chem.* **30**, 2785–2791 (2010).
87. Laskowski, R. A. & Swindells, M. B. LigPlot+: Multiple ligand-protein interaction diagrams for drug discovery. *J. Chem. Inf. Model.* **51**, 2778–2786 (2011).
88. Ihaka, R. & Gentleman, R. R: A Language for data analysis and graphics. *J. Comput. Graph. Stat.* **5**, (1996).

Acknowledgements

N.S. is supported by NSF-CAREER (Award #2047396) and NSF-EAGER (Award #2028283). This work is also supported by the CHARM3AT Labex program (ANR-11-LABX-39) to F.-D.B.; by AgreenSkills from the European Union in the framework of the Marie-Curie FP7 COFUND People Programme and a fellowship from Saclay Plant Sciences (ANR-17-EUR-0007) to A.d.S.G.; and by the Emmy Noether program (GU1423/1-1) of the Deutsche Forschungsgemeinschaft (DFG) to C.G. Furthermore, this work was supported by the Institut Jean-Pierre Bourgin's Plant Observatory technological platforms. We thank the beamline staff at the Advanced Light Source (U.S. DOE Office of Science User Facility under Contract No. DE-AC02-05CH11231, is supported in part by the ALS-ENABLE program funded by the National Institutes of Health, National Institute of General Medical Sciences, grant P30 GM124169-01). We thank the facilities and expertise of the I2BC proteomic platform (Proteomic-Gif, SICaPS) supported by IBiSA, Ile de France Region, Plan Cancer, CNRS and Paris-Sud University

Author contributions

AM.G., S.T., F.-D.B., C.R., C.G., A.dS.G., and N.S. conceived and designed the experiments. N.S., A.dS.G., and AM.G. conducted the protein purification, biochemical and crystallization experiments. J.-P.P. characterized pea Tilling mutants. S.T. performed pea RT-qPCR and root hair assay. P.LB. obtained Arabidopsis complementation lines. A.B., M.D. and C.LS. generated pea TILLING mutant collection. D.C. performed the mass experiments. N.S. and AM.G. determined and analyzed crystal structures and conducted in silico studies. S. T. performed pea root hair assays and gene expression analysis in Fig. 2. AM.G., A.dS.G., and N.S. wrote the manuscript with help from S.T., F.-D.B., C.R. and C.G.

Competing interests

The authors declare no competing interests.

Additional information

Supplementary information The online version contains supplementary material available at https://doi.org/10.1038/s42003-022-03085-6.

Correspondence and requests for materials should be addressed to AlexandredeSaint Germain or Nitzan Shabek.

Peer review information *Communications Biology* thanks Li Chen and the other, anonymous, reviewers for their contribution to the peer review of this work. Primary Handling Editor: Caitlin Karniski.

Reprints and permission information is available at http://www.nature.com/reprints

Publisher's note Springer Nature remains neutral with regard to jurisdictional claims in published maps and institutional affiliations.